

FME HYDROGENi

Deliverable D2.3.5: Current understanding and knowledge gaps for operation of hydrogen gas export compression systems

Organisation:	SINTEF Energy AS
Author(s):	Åsmund Ervik, Martin Spillum Grønli
Type of deliverable:	Memo
Sub-Project No:	SP2.3 Maritime and pipeline transportation
Deliverable No:	2.3.5
Issue Date:	October 2023
Number of pages:	40

SUMMARY:

This memo addresses compression of hydrogen for long-distance transport in pipelines, comparing existing and future expected pipelines for transport of hydrogen. With the focus to describe the working principles of centrifugal compressors authors also document a compressor performance code for future research and development. The code can import compressor performance maps and be used in compressor testing in accordance with the ASME PTC 10 standard.

KEYWORDS:

hydrogen pipelines, centrifugal compressor, single-stage compressor

<i>Dissemination Level</i>		
PU	Public	
RE	Restricted, for Consortium Parties only	X

Author(s): Åsmund Ervik, Martin Spillum Gnønli	Approved by WP Leader	<input checked="" type="checkbox"/>
Reviewer(s): Victoria Gribkovskaia	Name:	Victoria Gribkovskaia
Adm. Petter Nekså	Date:	31.10.2023
Responsible:	Signature:	



1 Introduction

Replacing fossil energy sources, such as natural gas, with hydrogen is seen as an important step towards reducing greenhouse gas emissions towards 2030 and beyond. The aim of this work is to give an introduction to compression of hydrogen for pipeline transportation over distances considerably longer than existing hydrogen pipelines are designed for. Because of pressure loss in the pipeline system, compressors must provide high discharge pressures. Although hydrogen has high *gravimetric* energy density, it has low *volumetric* energy density due to low molar weight. Table 1 gives a comparison of different properties of hydrogen (H_2) and methane (CH_4) gas, where the latter typically constitutes 85–90 % of natural gas. Replacing natural gas with hydrogen and delivering the same amount of energy from pipelines stresses the need for compressors with high discharge pressures as well as high mass flow rates. The pressure in existing and proposed hydrogen pipelines are often set to around 100 barg (gauge pressure). For longer pipelines relevant to Norwegian export of hydrogen, this may be raised to 200 barg, along with a higher mass flow rate. We will therefore review both pressure alternatives, where the lower pressure alternative is discussed in greater detail in the literature. Due to large flow rates, it is probable that hydrogen compressor trains will involve centrifugal compressors, which belong to the category of dynamic compressors. A focus of this work is therefore to describe the working principles of centrifugal compressors. An important standard in this context is the American Petroleum Institute (API) standard 617 for axial and centrifugal compressors and expander-compressors.

We start out by presenting a general introduction to both centrifugal and axial compressors. Next, we give an introduction to the stage dynamics of centrifugal compressors. This includes describing how pressure rise is achieved for different types of centrifugal compressor configurations and how unwanted flow separation can arise. In addition, we outline how the required compressor work can be calculated using different approaches. Subsequently, state of the art for high-capacity hydrogen compression is presented. Finally, we present an open-source Python code that allows to calculate the performance of centrifugal compressors.

Table 1: Properties of hydrogen (H_2) and methane (CH_4) gas at 1 bar and 15 °C.

Property	Hydrogen (H_2)	Methane (CH_4)
Molecular weight [g/mol]	2.016	16.043
Density [kg/m ³]	0.084	0.671
Volumetric energy density [MJ/m ³]	10.2	37.3
Gravimetric lower heating value [MJ/kg]	120	56
Thermal conductivity [W/mK]	0.18	0.033
Critical pressure [bar]	13	47
Critical temperature [°C]	-240	-83
Autoignition temperature [°C]	500	580



SINTEF

2 Dynamic compressors

In this chapter we will give a basic introduction to dynamic compressors. Another category of compressors is the reciprocating compressors. These are also called piston compressors and use a piston to compress gas within a trapped volume. On the other hand, dynamic compressors operate by increasing the momentum of a gas as it flows through them. Dynamic compressor can be divided into two categories:

1. Axial compressors
2. Centrifugal (radial) compressors

Next, centrifugal compressors are often divided into three categories:

1. Horizontally split
2. Vertically split (barrel type)
3. Integrally geared

Centrifugal compressors are in particular relevant for hydrogen compression as they allow for higher discharge pressures than axial compressors. However, they require several stages with a large footprint to reach the needed pressure ratios. To get an overview, we present an intro to both axial and centrifugal compressors. It can be mentioned that reciprocal compressors are typically selected for low to medium volume flows that require high pressure ratios. Although reciprocal compressors typically have a higher maintenance requirement, using several reciprocal compressors in parallel may be an option for hydrogen compression. As we will see, the horizontally split centrifugal compressors are not relevant for pressures needed for hydrogen pipeline export. Thus, we are interested in vertically split and integrally geared centrifugal compressors.

2.1 Centrifugal compressors

Centrifugal compressors (also called radial or impeller compressors) resembles a centrifugal pump and gives a relatively large pressure gradient per step when the peripheral speed is large (achieving a high Mach number). Figure 1 shows a photograph of a centrifugal compressor with a cutout. The fluid approaches the suction side axially from the left with low speed. The impeller rotates and flings the fluid radially outwards in all directions as indicated by the green streamlines, increasing the speed and temperature of the fluid. The diffuser changes the direction of the radially moving fluid, and has an increasing cross-section that converts the kinetic energy into increased static pressure (potential energy), by slowing (diffusing) the fluid velocity.

Centrifugal compressors are probably the second most used compressors in the process industry today, only behind reciprocating compressors. Different classifications of centrifugal compressors are shown in Table 2. Centrifugal compressors can consist of one or more stages. A stage is defined as a pair of an impeller and a diffuser. A process stage is a block that consists of one or more uncooled stages. Coolers between process stages (intercoolers) are used to limit the temperature rise such that the necessary compression power is kept at a minimum.

Compressors can also have different types of casing. A horizontal split allows removal of only the upper half for maintenance, without disturbing the process piping. However, when the partial pressure of hydrogen at the casing exceeds 14.0 bar, the API standard 617 recommends vertical split casing. Furthermore, a double flow configuration can be used for large volumetric flow rates, which are usually associated with low inlet pressures. To allow for even higher pressures and flow rates, integrally geared compressors may be utilized. These are multi-shaft machines where each impeller operates at its optimum speed.

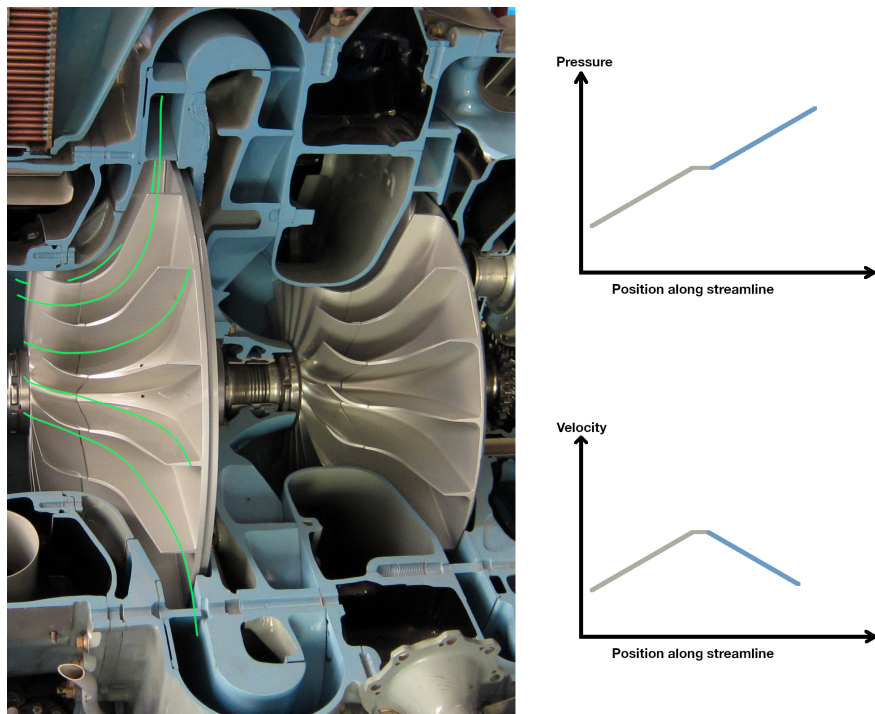


Figure 1: A photograph of a two-stage centrifugal compressor with impeller in silver and diffuser in blue, with streamlines indicated by the green lines. On the right side, the pressure and velocity along a streamline is indicated as the flow goes from the impeller (silver) to the diffuser (blue). Adapted from public domain photo.

A centrifugal compressor is often limited by how big it can be made and how fast the impeller can rotate before it disintegrates. An impeller with large radius requires high circumferential speed. Below we have summarized a collection of pros and cons for centrifugal compressors.

Pros:

- Simplicity of manufacturing and relatively low cost since it requires fewer stages to give the same pressure rise as an axial compressor.
- Higher pressure gradient than a single-stage axial compressor. A multi-stage axial compressor can be followed by a single-stage centrifugal compressor in order to minimize the length of the compressor and diameter of the centrifugal compressor.
- Few rubbing parts and relatively energy efficient. Gives higher and non-oscillating constant flow compared to reciprocating compressors of the same size.

Cons:

- Cannot achieve the high compression ratios of reciprocating compressors without multiple stages.
- High weight and stress, and large frontal area because of the large diameter of the radial diffuser.
- Changing the flow direction several times results in energy loss.



Table 2: Classification of centrifugal compressors based on the listing in Ref. [1].

Number of stages	Single	Overhung
		Between bearing
Process	Multi	Integrally geared
		Between bearing
Design of casing	Single process stage	... with back-to-back impellers
		With side streams
Flow direction	Multi-process stage	Integrally geared
		Without intercooling
Casing split	Single casing	With intercooling
	Double casing	
Arrangement	Single flow	
	Double flow	Two inlets
		Flow split integrally
	Horizontal	
	Vertical	
	Horizontal	
	Vertical inline	

2.2 Axial compressors

Axial compressors are not expected to be relevant for hydrogen compression. Nonetheless, some of the working principles overlap with those of centrifugal compressors implying that a basic understanding of axial compressors may be rewarding. Axial compressors resemble a series of axial fans on the same axis. A photograph of a single-spool axial compressor typically used in jet-engines is shown in Figure 2 (next page). It consists of rotating airfoil-shaped blades that are attached peripherally to a central rotating drum. Stationary vanes (stators) are placed in-between the rotating blades (rotors). The stators are mounted on the compressor casing. Furthermore, a stage refers to one rotor-stator pair. All blades can in principle be varied dynamically making it possible to adapt to varying operating conditions such as decreased mass flow.

The variation in fluid pressure and velocity inside an axial compressor is similar to the variations in a centrifugal compressor, with a steady increase in pressure, and the velocity alternating between increasing in the rotor sections and decreasing in the stator sections. Rotors spin and accelerate the fluid in both the axial and circumferential directions, pushing it towards the stators. The stators convert the increased kinetic energy into static pressure by diffusion. In addition, they channel the fluid towards the next stage of rotor-stator blades. To maintain an optimal axial velocity as the fluid is compressed, the cross-sectional area between compressor casing and rotor drum is reduced in the axial (flow) direction. Axial compressors are often limited by the accompanying temperature rise.



SINTEF



Figure 2: A photograph of an axial compressor section of a jet engine, where the rotors can be seen, as well as the welds indicating the position of the stator blades. Public domain image.



SINTEF

3 Centrifugal compressor characteristics

Centrifugal compressors are limited by several phenomena and some of them are described in the following. Figure 3 shows a typical compressor performance map. In this, the compressor efficiency is a measure of how efficient the compression process is compared to an adiabatic compression. Constant efficiency is depicted by so-called efficiency islands.

Surging is a phenomenon that limit compressors. It arises when the flow rate is too low compared to the compressors ideal operating conditions resulting in intermittent flow reversal. It can damage the whole operating cycle including the compressor driver, rotor bearings and rotor seals, resulting in high vibrations and high temperatures. The compressor performance map in Figure 3 shows how surge and the associated surge cycle can arise. First, assume that the compressor operates at point A (p_A, \dot{m}_A) on the characteristic curve (where the rotational speed is constant). Reducing the flow rate to \dot{m}_B by closing a control valve on the delivery pipe will result in increased static pressure upstream of the valve. This is matched by an increased delivery pressure. The same process will happen reducing the flow rate to \dot{m}_C and \dot{m}_S on the characteristic curve.

However, reducing the flow rate even further will instead reduce the pressure ratio, implying an unbalance between the pipe pressure and delivery pressure. The resulting reversed flow breaks down the normal steady flow, pressure falls and the compressor recovers its normal stable operation at point B with a flow rate \dot{m}_B . Nevertheless, the control valve is still adjusted for a flow rate $\dot{m}_D < \dot{m}_B$. The surge cycle EBCSDE will therefore repeat itself and may cause serious damage to the compressor due to reversed flow.

Another phenomena is compressor choking or stonewalling which happens when the flow rate through the compressor cannot be increased further since some part of the compressor has reached a Mach number of unity. Stalling is yet another phenomena that limits operation of compressors. If the flow separates from the compressor blade, stalling is said to occur. This causes a reduced pressure ratio and can lead to reversed flow. It can be mentioned that having a Mach number greater than unity is perfectly possible inside some parts of the compressor.



SINTEF

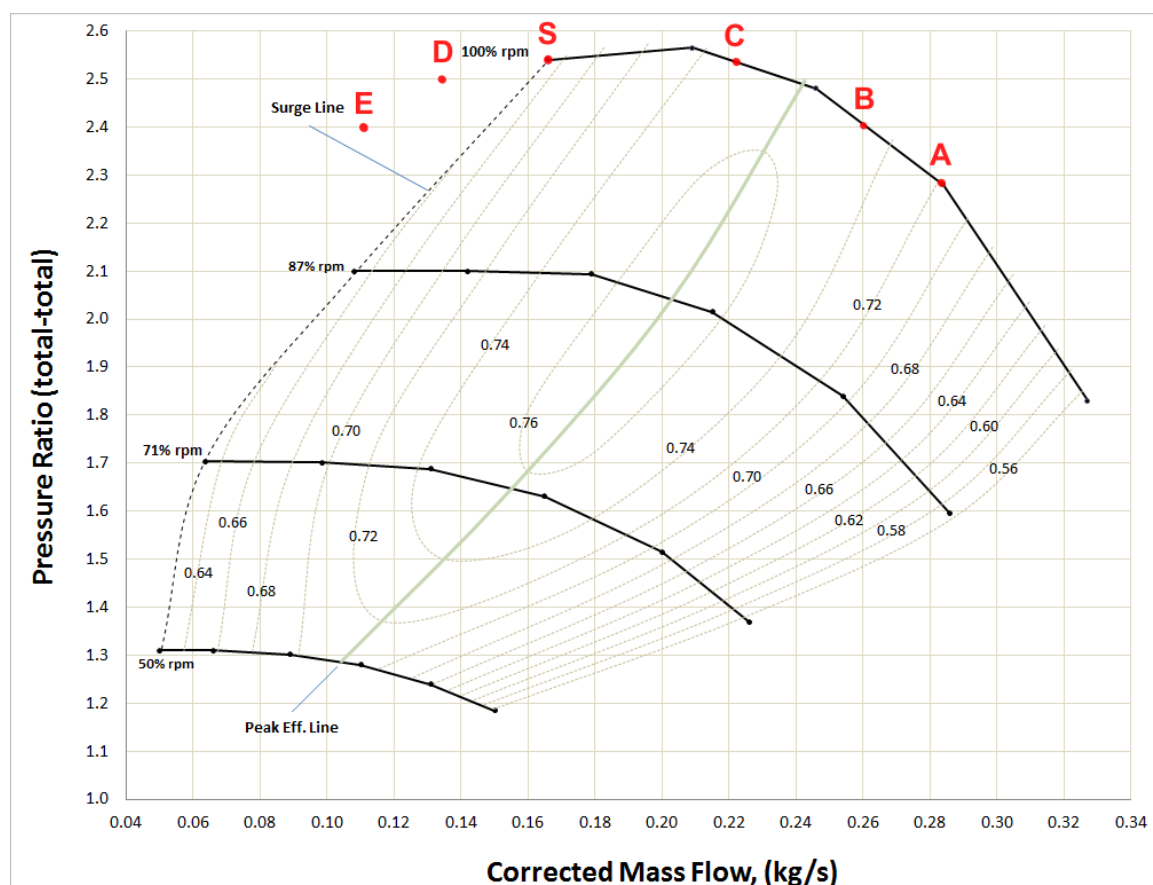


Figure 3: Typical compressor performance map. Public domain figure.



SINTEF

4 Centrifugal compressor stage dynamics

We will in the following give an introduction to the stage dynamics of centrifugal compressors for various design options. Operation with higher molecular weight gases is often limited by the Mach numbers. For instance can an inlet Mach number of unity cause choking. However, for low molecular weight gases like hydrogen, the operation is instead primarily limited by mechanical strength. The impeller tip speed is significantly influenced by the desired overall pressure ratio. Moreover, the maximum allowable speed, determined by mechanical strength, can vary depending on the specific materials used for the impeller. Together with the complications of hydrogen embrittlement, this is important to keep in mind when designing a hydrogen compressor.

The centrifugal compressor in Figure 1 shows how gas enters the inducer with an axial velocity. The inducer turns the relative flow as it enters the impeller passages. Here, the impeller exit has straight blades in the radial direction. These can also be forward or backward leaning as we will discuss later. After leaving the impeller, the gas passes through a radial diffuser in which momentum is exchanged for pressure. A radial diffuser can consist of a vaneless portion succeeded by a series of stator vanes. The gas leaving the diffuser is collected and delivered to the outlet.

To understand the dynamics in greater detail, we start out by calculating the compressor torque and work as a function of rotational speed. In addition, we relate the compressor work to enthalpy rise. Next, we examine how centrifugal and axial compressors achieve pressure rise in different ways. Subsequently, we derive an expression for the pressure rise taking impeller blade geometry and adiabatic efficiency into consideration. The Mach number at the impeller exit is also calculated. Thereafter, we study how unwanted boundary layer separation can occur in the inducer and at the impeller exit. An expression for the maximal rotational speed of the impeller is then obtained. Ultimately, we determine the dimensions of a radial diffuser with a vaneless region and a region with vanes.

The following sections are based on the exposition in [2]. This book is freely available from <https://archive.org/details/MechanicsAndThermodynamicsOfPropulsionHillPeterson>. Several figures from the book are thus reproduced here.

4.1 Torque in a centrifugal compressor

To understand the working principles of a centrifugal compressor, it is useful to examine the energy equation for a streamline passing through the rotor. This can for instance be used to calculate the total shaft work required to drive the compressor. The sum of torques applied to a control volume surrounding a single compressor rotor is

$$\sum \tau = \dot{m} [(rc_\theta)_2 - (rc_\theta)_1], \quad (1)$$

where the subscripts 1 and 2 represents the compressor inlet and outlet, respectively. Moreover, \dot{m} is the mass flow rate through the compressor, r is the radius and c_θ is the tangential velocity. To show this relation we must examine the angular momentum inside a centrifugal compressor. Consider a single particle of fluid of mass δm moving with a radial, tangential and axial particle velocity c_r , c_θ and c_z . We choose a cylindrical coordinate system (r, θ, z) for convenience. The angular momentum of the particle about the z -axis is $\delta m r c_\theta$. We write Newton's second law for the particle as

$$\mathbf{F} = \delta m \frac{d\mathbf{c}}{dt}, \quad (2)$$

where

$$\mathbf{F} = \mathbf{r} F_r + \theta \mathbf{F}_\theta + \mathbf{z} F_z, \quad \mathbf{c} = \mathbf{r} c_r + \theta c_\theta + \mathbf{z} c_z,$$

in which $(\mathbf{r}, \theta, \mathbf{z})$ are unit vectors in the radial, tangential and axial directions. Even though the magnitudes of the unit vectors remain constant, the direction of \mathbf{r} and θ may change with time so that

$$\frac{d\mathbf{r}}{dt} = \theta \frac{d\theta}{dt} \quad \text{and} \quad \frac{d\theta}{dt} = -\mathbf{r} \frac{d\theta}{dt}. \quad (3)$$

Writing out the three components of Eq. (2) then yields

$$\begin{aligned} \mathbf{r}: \quad F_r &= \delta m \left(\frac{dc_r}{dt} - c_\theta \frac{d\theta}{dt} \right), \\ \theta: \quad F_r &= \delta m \left(\frac{dc_\theta}{dt} - c_r \frac{d\theta}{dt} \right), \\ \mathbf{z}: \quad F_r &= \delta m \left(\frac{dc_z}{dt} \right). \end{aligned} \quad (4)$$

Multiplying the θ -component by r yields

$$rF_\theta = \delta m \left(r \frac{dc_\theta}{dt} + c_r r \frac{d\theta}{dt} \right) = \delta m \frac{d}{dt}(rc_\theta), \quad (5)$$

where we utilized that $c_r = dr/dt$ and $c_\theta = r(d\theta/dt)$. The product rF_θ is defined as the torque on the particle with respect to the z -axis. The angular momentum rc_θ per unit mass about a given axis is therefore constant if no torque is applied.

When dealing with fluids it is often more convenient to write Newton's laws as they apply to control volumes instead of particular portions of matter. We must therefore transform Eq. (5) into a form that is applicable to a control volume. It can be shown that the total torque $\sum \tau$ acting on the control volume (CV) reads

$$\sum \tau = \frac{d}{dt} \int_{CV} \rho r c_\theta dV + \int_{CS} \rho r c_\theta (\mathbf{c} \cdot \mathbf{n}) dA, \quad (6)$$

where the unit vector \mathbf{n} points outward from the control surface (CS). The first term represents the rate of change of angular momentum stored within the control volume. The second term represents the net outward flux of angular momentum from that control volume.

Figure 4 shows a control volume for a dynamic compressor that encloses a single row of rotating blades mounted on a disc and shaft. The control volume includes inlet and outlet flow areas, and a cylindrical surface that is located at the tip diameter of the rotor housing. The blades rotate with an angular velocity Ω and can be of any shape. The flow inside a turbomachine rotor is unsteady and asymmetric relative to the control surface. However, the unsteadiness is periodic with a high frequency implying that, on average, the time-dependent term in Eq. (6) can be omitted, resulting in

$$\sum \tau = \int_{CS} \rho r c_\theta (\mathbf{c} \cdot \mathbf{n}) dA. \quad (7)$$

Since the blade exerts force on the flow, there must be some tangential variations of fluid pressure and velocity between the blades *inside* the control volume. However, upstream and downstream of the rotor, these variations can be neglected. Because the control volume completely encloses the rotor, we can assume that flow across the inlet and outlet surfaces is axisymmetric and steady. The integral over the control surface in the above equation will therefore not be affected by asymmetric flow, nor unsteady flow.

The components of the fluid velocity can vary significantly in the radial direction. To show Eq. (1), we will first consider only an increment of flow rate that enters the control volume through an incremental area having

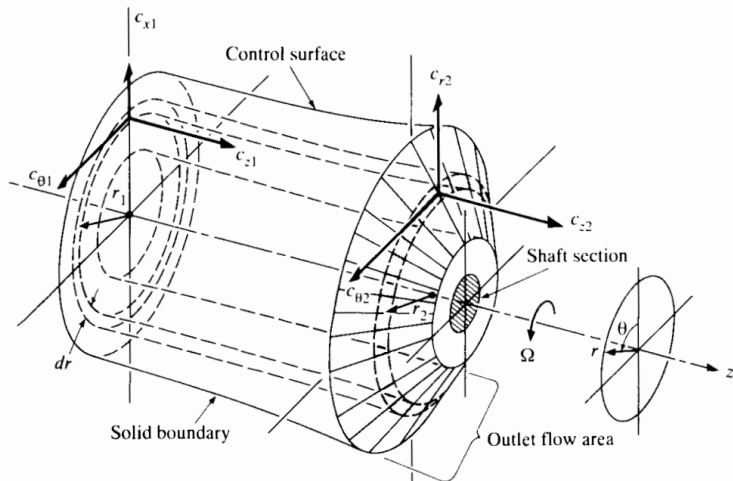


Figure 4: Control volume for axisymmetric flow entering and leaving a rotor. Applicable to both axial and centrifugal compressors. Figure reproduced from [2].

mean radius r_1 and radial width dr as illustrated in Figure 4. This flow will occupy a cylindrical annular stream tube and leave the control volume at a mean radius r_2 . Hence, we take c_z , c_r and c_θ to be independent of r and θ at the inlet and outlet. Furthermore, Eq. (7) requires that the incremental torque is proportional to the mass flow rate times the change in fluid angular momentum per unit mass, leaving us with

$$d\tau = d\dot{m}(r_2 c_{\theta 2} - r_1 c_{\theta 1}), \quad (8)$$

where $d\tau$ is the sum of the torques which act on the inlet and outlet surfaces of the angular stream tube. Summing over the full inlet and outlet areas yields

$$\sum \tau = \int_{A_2} (rc_\theta) \rho c_n dA - \int_{A_1} (rc_\theta) \rho c_n dA, \quad (9)$$

in which c_n is the component of velocity normal to the area dA . Having a free-vortex flow where rc_θ is a constant or taking a "suitable average", we can integrate the above equation to

$$\sum \tau = \dot{m} [(rc_\theta)_2 - (rc_\theta)_1], \quad (10)$$

which is the result in Eq. (1) we wanted to show. This equation can be used to give rough estimates of the required work or power to drive the compressor.

To that end, we assume that the total torque is equal to the torque τ_s applied by the shaft to the rotor. This allows us to express the total work per unit mass done by the rotor on the gas as

$$w = \Omega \tau_s / \dot{m} = \Omega (rc_\theta)_2 - \Omega (rc_\theta)_1 \quad (11)$$

or

$$w = (U c_\theta)_2 - (U c_\theta)_1, \quad (12)$$

where $U = \Omega r$ and Ω is the rotational speed of the shaft. It may not be true that all streamlines passing through a rotor undergo the same change in angular momentum. However, Eq. (12) can be thought of as applying to a given streamline.



SINTEF

4.2 Total work and stagnation enthalpy

In this section, we will show an alternative way to arrive at the required compressor work. We start out by defining the *stagnation state* as the state that is reached if a fluid is brought to rest reversibly, adiabatically and without work. The stagnation state will from now on be denoted by a subscript 0. By neglecting gravitational and other body forces, it is then possible to show that the work done on the fluid equals the stagnation enthalpy increase for steady-flow adiabatic compression. The first law of thermodynamics states that

$$dE = \delta Q - \delta W, \quad (13)$$

where dE denotes the change in internal energy of a closed system, δQ is the supplied heat to the system and δW is the amount of thermodynamic work done by the system on its surroundings. We choose a control volume enclosing a steady-state system where the mass flow rate $\dot{m}_{\text{in}} = \dot{m}_{\text{out}} = \dot{m}$, such that

$$\frac{dE_{\text{CV}}}{dt} = \dot{Q}_{\text{CV}} - \dot{W}_{\text{CV}} + \dot{m}(e_{\text{in}} - e_{\text{out}}), \quad (14)$$

where the last term represents the rate at which energy flows in and out of the control volume. Here we have $\dot{Q} = \lim_{dt \rightarrow 0} (\delta Q/dt)$ and $\dot{W} = \lim_{dt \rightarrow 0} (\delta W/dt)$.

Hence, in a steady-state we know that

$$\dot{Q}_{\text{CV}} - \dot{W}_{\text{CV}} = \dot{m}(e_{\text{out}} - e_{\text{in}}) = \dot{m}[(IE + KE + PE + CE)_{\text{out}} - (IE + KE + PE + CE)_{\text{in}}]. \quad (15)$$

Neglecting potential and chemical energy (PE and CE), and keeping only the internal and kinetic energy (IE and KE) leaves us with

$$\dot{Q}_{\text{CV}} - \dot{W}_{\text{CV}} = \dot{m} \left[\left(u + \frac{c^2}{2} \right)_2 - \left(u + \frac{c^2}{2} \right)_1 \right], \quad (16)$$

in which u is the internal energy per unit mass and c is the absolute fluid velocity. Subscripts 1 and 2 denotes the inlet and outlet of the control volume as previously. Dividing by mass flow and separating the work into flow work done by the system $p_2v_2 - p_1v_1$ and external/shaft work w done on the system yields

$$q + w = (u_2 + p_2v_2) - (u_1 + p_1v_1) + \frac{c_2^2}{2} - \frac{c_1^2}{2}, \quad (17)$$

or

$$q + w = h_2 - h_1 + \frac{c_2^2}{2} - \frac{c_1^2}{2}, \quad (18)$$

where h is the enthalpy per unit mass. Here, the positive sign in front of w originates from defining the shaft work as positive, even though the work is performed on the system. Finally, for an adiabatic process we find that the total work equals the increase in stagnation enthalpy,

$$w = h_{02} - h_{01} = h_2 - h_1 + \frac{c_2^2}{2} - \frac{c_1^2}{2}. \quad (19)$$

The stagnation enthalpy $h_0 = h + c^2/2$. Eq. (12) can then be cast into

$$h_2 - h_1 = (Uc_\theta)_2 - (Uc_\theta)_1 - \frac{c_2^2}{2} + \frac{c_1^2}{2}. \quad (20)$$



SINTEF

4.3 Pressure rise

In order to understand how pressure is increased in a centrifugal compressor, we move to a reference frame fixed to the rotor. We introduce notation for the absolute velocities c and relative velocities w :

$$\begin{aligned} c_\theta &= U + w_\theta, \\ c_r &= w_r, \\ c_z &= w_z, \\ c^2 &= c_r^2 + c_\theta^2 + c_z^2, \\ w^2 &= w_r^2 + w_\theta^2 + w_z^2, \end{aligned} \tag{21}$$

Eq. (20) can then be written as

$$h_2 - h_1 = \frac{U_2^2}{2} - \frac{U_1^2}{2} - \left(\frac{w_2^2}{2} - \frac{w_1^2}{2} \right). \tag{22}$$

This can be called the energy equation for a frame of reference fixed to the rotor. It applies to a streamline observed in the same reference frame. Considering an increment along the streamline gives

$$dh = d\left(\frac{\Omega^2 r^2}{2}\right) - \frac{dw^2}{2}. \tag{23}$$

Exploiting the relation $Tds = dh - dp/\rho$ leaves us with

$$\frac{dp}{\rho} = d\left(\frac{\Omega^2 r^2}{2}\right) - \frac{dw^2}{2} - Tds. \tag{24}$$

For isentropic flow, this turns into

$$\frac{dp}{\rho} = d\left(\frac{\Omega^2 r^2}{2}\right) - d\left(\frac{w^2}{2}\right). \tag{25}$$

We note that an axial compressor will have $dr \simeq 0$ along a streamline. This implies that in an axial compressor, pressure rise can only be obtained by deceleration of the flow, i.e. having a change in the relative velocities. On the other hand, centrifugal compressors can achieve pressure rise even if there are no change in relative velocity w . This is advantageous because relative velocities can cause boundary layer separation where the fluid separates from the surface into a wake, limiting the operation of the compressor. In other words, centrifugal compressors are not limited by boundary layer separation in the same way as axial ones are. Higher stage pressure ratios are therefore achievable in centrifugal compressors. Having that said, boundary layer separation can still limit the design of centrifugal compressors, something that is discussed in sections 4.5 and 4.6.

4.4 Impeller blade geometry and total pressure rise

To study the effects of different impeller blade geometries on pressure rise and exit Mach number, we examine the work done by the centrifugal compressor rotor depicted in Figure 5. For simplicity we assume equal angular momentum, (rc_θ) , for all streamlines. Centrifugal compressors do often have swirl-free inlet flow, but others have swirl at the inlet because of inlet guide vanes positioned before the rotor entrance. Swirl can also arise from a compressor stage upstream. However, with uniform swirl upstream and downstream, we can rewrite Eq. (12) as

$$w = c_p(T_{02} - T_{01}) = U_2 c_{\theta 2} - U_1 c_{\theta 1}, \tag{26}$$

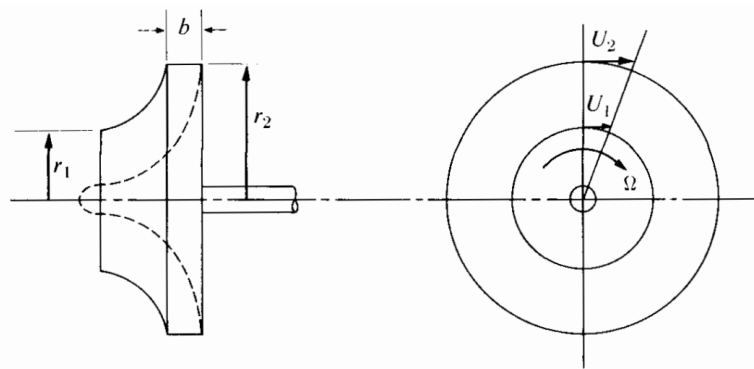


Figure 5: Centrifugal compressor rotor. Figure reproduced from [2].

where T_{01} and T_{02} are the stagnation temperatures at entrance to and exit from the rotor, respectively. In this we have assumed ideal gas behaviour such that the specific heats per unit mass at constant pressure and volume are related as $c_p - c_v = R$ and $c_p/c_v = \gamma$, where R is the gas constant. Dividing the work by $c_p T_{01}$ we find

$$\frac{T_{02} - T_{01}}{T_{01}} = (\gamma - 1) \left(\frac{U_2}{a_{01}} \right)^2 \left[\frac{c_{\theta 2}}{U_2} - \frac{(U c_{\theta})_1}{U_2^2} \right], \quad (27)$$

where $a_{01} = \sqrt{\gamma R T_{01}}$ is the speed of sound at the inlet stagnation temperature. Three standard types of blading in a centrifugal compressor rotor are shown in Figure 6 together with the velocity triangles in the radial plane at the outlet of each type. The different bladings are straight radial blading, backward leaning blading and forward leaning blading. All rotors are shown with the same tip speed U_2 and radial velocity component $w_r = c_r$. At first we assume the relative fluid velocity leaving the impeller to be parallel to the blade. We define β_2 as the angle of exit relative velocity with respect to the radial direction. A backward leaning blade has a positive β_2 . The relative and absolute velocity components w_r and c_r are equal since the rotor speed U is entirely tangential.

A machine with purely axial inlet velocity will reduce Eq. (27) to

$$\begin{aligned} \frac{T_{02} - T_{01}}{T_{01}} &= (\gamma - 1) \left(\frac{U_2}{a_{01}} \right)^2 \frac{c_{\theta 2}}{U_2} \\ &= (\gamma - 1) \left(\frac{U_2}{a_{01}} \right)^2 \left(1 - \frac{w_{r2}}{U_2} \tan \beta_2 \right), \end{aligned} \quad (28)$$

where we used that the three types of impeller blading all have $c_{\theta 2} = U_2 - w_{r2} \tan \beta_2$. In addition, continuity gives

$$w_{r2} = \frac{\dot{m}}{2\pi r_2 b \rho_2}, \quad (29)$$

in which b is the blade height at exit and ρ_2 is the exit density. The blade height is the height of the blade out of the radial plane. The dependency on the exit blade angle will, for an increasing mass flux, give an increase in stagnation temperature rise for forward-leaning blades. For backward-leaning blades, the stagnation temperature rise will decrease with increasing mass flux, while it remains constant for straight radial blades. From Eq. (26) we have that work done by the rotor on the fluid is related to the stagnation temperature rise. Therefore, at the same tip speed U_2 and mass flow rate \dot{m} , rotors with forward-leaning blades will do more work on the fluid, and one can expect higher pressure rise compared to rotors with straight radial or

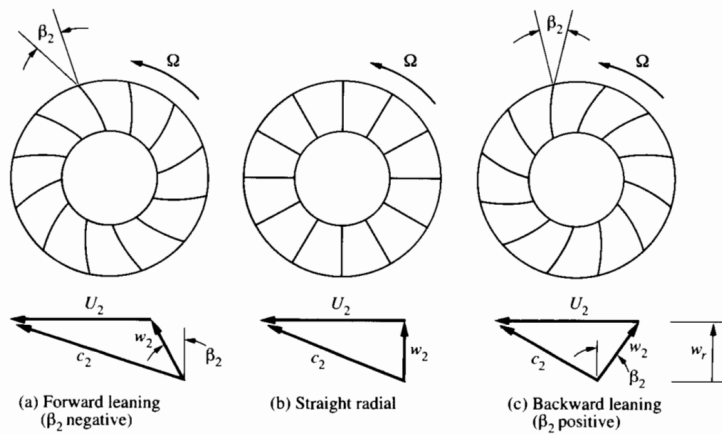


Figure 6: Shapes of centrifugal impeller blades and corresponding outlet velocity triangles. Figure reproduced from [2].

backward-leaning blades. On the other hand, output pressure tends to rise with increasing mass flow rate for compressors with forward-leaning blades. This trend is associated with dynamic instability. Forward-leaning blades are consequently not used in aircraft engines.

By comparing radial blades with backward-leaning blades, we see that radial blades are capable of higher pressure rise for a given tip speed. However, because $c_{\theta 2} = U_2 - w_{r2} \tan \beta_2$, the Mach number of the fluid entering the diffuser is also higher for radial blades. A challenge with backward-leaning blades is the bending-stress problem, although different design alternatives can be chosen to circumvent this problem. Moreover, stronger materials are being developed allowing for high tip speed operation. This is a key R&D challenge for hydrogen compressors which require high tip speeds.

To find the overall stagnation pressure ratio of a stage, p_{03}/p_{01} , we start out by defining the stage adiabatic efficiency as

$$\eta_c = \frac{h_{03s} - h_{01}}{h_{03} - h_{01}}, \quad (30)$$

where the subscript 03s denotes the diffuser exit stagnation state reached after an isentropic compression. The subscript 03 denotes the same but for an actual compression, not isentropic. The enthalpy differences are found by exploiting that $dh = c_p dT$ for an ideal gas. Thus, the adiabatic efficiency becomes

$$\eta_c = \frac{T_{03s} - T_{01}}{T_{03} - T_{01}}. \quad (31)$$

Stagnation temperatures such as T_{03} and T_{01} are easily measured. What remains is therefore to calculate the stagnation temperature T_{03s} obtained by an isentropic process and relate it to the pressure rise of the compressor stage.

We do so by noting that $dq = de + dw$. In addition, for a reversible process we know that $ds = (dq/T)_{rev}$. Since $dw = pdv$, this gives us

$$Tds = de + pdv. \quad (32)$$

Next, we insert $h = e + pv$, such that

$$Tds = dh - vdp. \quad (33)$$

An ideal gas has $dh = c_p dT$ and $pV = RT$. We can therefore write

$$\frac{ds}{R} = \frac{\gamma}{\gamma-1} \frac{dT}{T} - \frac{dp}{p}. \quad (34)$$

Hence, the temperatures T_{03s} and T_{01} , which are related by an isentropic process, is given by

$$\frac{T_{03s}}{T_{01}} = \left(\frac{p_{03s}}{p_{01}} \right)^{\frac{\gamma-1}{\gamma}}. \quad (35)$$

The adiabatic efficiency in Eq. (30) can then be manipulated into a relation between the overall pressure ratio for a stage and the stagnation temperatures,

$$\frac{p_{03}}{p_{01}} = \left[1 + \eta_c \frac{T_{03} - T_{01}}{T_{01}} \right]^{\frac{\gamma}{\gamma-1}}. \quad (36)$$

Here, we have set $p_{03s} = p_{03}$ since the two thermodynamic processes starting from state 01 arrive at the same pressure, although the non-isentropic process requires more work. Having adiabatic flow in the diffuser lets us set $T_{03} = T_{02}$ which together with Eq. (28) yield the overall pressure ratio

$$\frac{p_{03}}{p_{01}} = \left[1 + \eta_c(\gamma-1) \left(\frac{U_2}{a_{01}} \right)^2 \left(1 - \frac{w_{r2}}{U_2} \tan \beta_2 \right) \right]^{\frac{\gamma}{\gamma-1}}. \quad (37)$$

Next, we want to determine the exit Mach number of the impeller for different blade geometries. The absolute Mach number M_2 at the exit of the impeller reads

$$M_2 = \frac{c_2}{a_2}. \quad (38)$$

By inspecting Figure 6 we find that the absolute exit velocity c_2 is given by

$$c_2^2 = (U_2^2 - w_{r2} \tan \beta_2)^2 + w_r^2. \quad (39)$$

Furthermore, the speed of sound at the rotor exit is

$$a_2^2 = \gamma R T_2 = a_{01}^2 \frac{T_{02}}{T_{01}} \left/ \left(1 + \frac{\gamma-1}{2} M_2^2 \right) \right.. \quad (40)$$

To show this one must recall that $dh = c_p dT$ and $c_p = \gamma R / (\gamma-1)$ for an ideal gas. Moreover, we have used that stagnation enthalpy $h_{02} = h_2 + c_2^2/2$ and $a_{01}^2 = \gamma R T_{01}$. Recalling Eq. (28), we find the stagnation temperature fraction to be

$$\frac{T_{02}}{T_{01}} = 1 + (\gamma-1) \left(\frac{U_2}{a_{01}} \right)^2 \left(1 - \frac{w_{r2}}{U_2} \tan \beta_2 \right). \quad (41)$$

Combining Eqs. (37) and (41), gives an expression for the Mach number at the exit of the impeller,

$$M_2 = \sqrt{\frac{A}{1 - \frac{\gamma-1}{2} A}}, \quad (42)$$

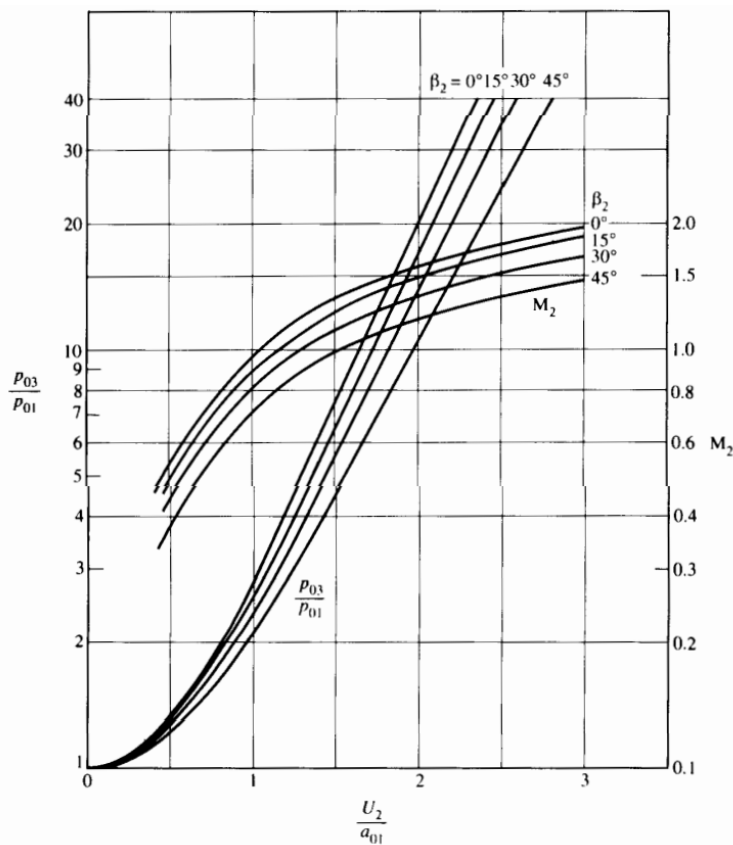


Figure 7: Left vertical axis shows the stagnation pressure rise in a centrifugal compressor stage for different relative velocity angles at rotor exit β_2 with adiabatic efficiency $\eta_c = 0.85$ and flow coefficient $w_{r2}/U_2 = 0.30$. Right vertical axis shows the absolute Mach number M_2 at the exit of the impeller for the same values of β_2 , η_c and w_{r2}/U_2 . The numerical values is calculated for air. Figure reproduced from [2].

in which the parameter A reads

$$A = \left(\frac{U_2}{a_{01}} \right)^2 \frac{\left[\left(1 - \frac{w_{r2}}{U_2} \tan \beta_2 \right)^2 + \left(\frac{w_{r2}}{U_2} \right)^2 \right]}{\left[1 + (\gamma - 1) \left(\frac{U_2}{a_0} \right)^2 \left(1 - \frac{w_{r2}}{U_2} \tan \beta_2 \right) \right]}. \quad (43)$$

The dependency of stage pressure rise and exit Mach number on the angle of relative exit velocity from the rotor β_2 and flow coefficient w_{r2}/U_2 is shown in Figures 7 and 8. The figures are obtained from Eqs. (36) and (42), and can be used to decide which Mach number a certain pressure rise will correspond to. This is important since supersonic velocities may limit the compressor operation, at least for gases having high molar mass.

4.5 Inducer and maximal rotational speed

The entrance section of the impeller is called an inducer. The inducer acts to change the tangential motion of the fluid with little or no radial acceleration. The radial velocity is much larger than the axial velocity only in



SINTEF

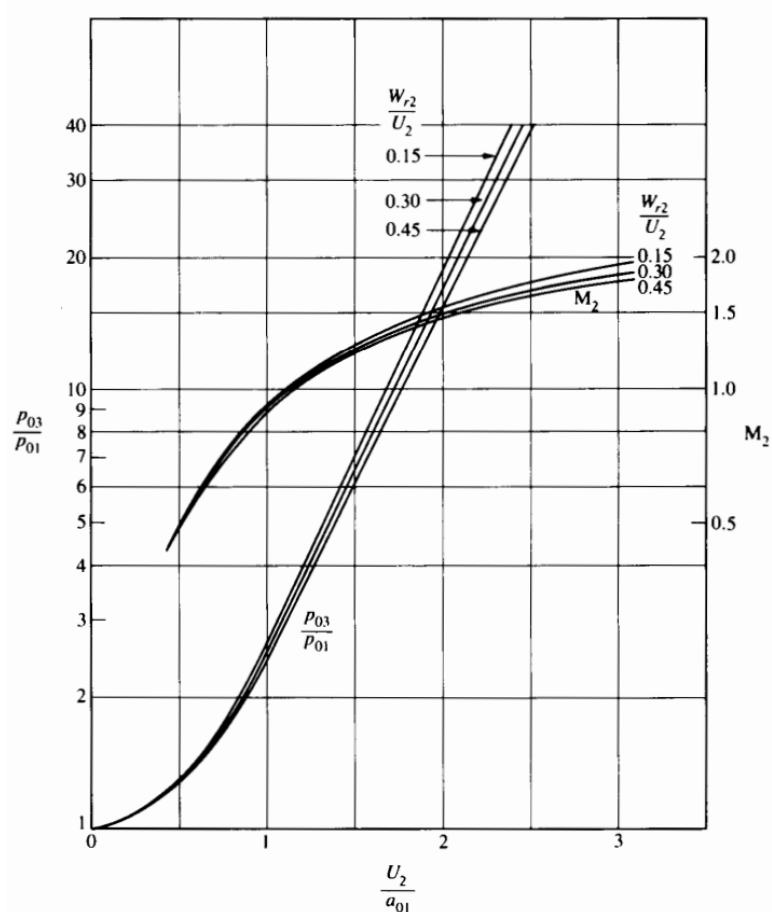


Figure 8: Left vertical axis shows the stagnation pressure rise in a centrifugal compressor stage for different flow coefficients w_{r2}/U_2 with adiabatic efficiency $\eta_c = 0.85$ and relative velocity angle at rotor exit $\beta_2 = 15^\circ$. Right vertical axis shows the absolute Mach number M_2 at the exit of the impeller for the same values of w_{r2}/U_2 , η_c and β_2 . The numerical values is calculated for air. Figure reproduced from [2].

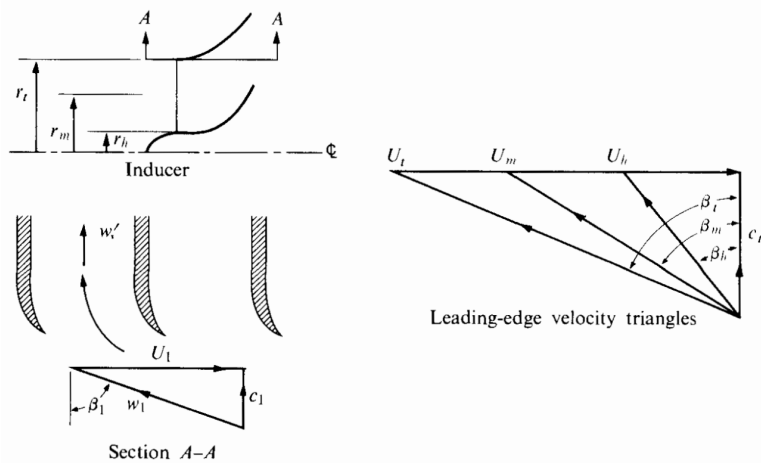


Figure 9: Diagram of an inducer inlet. Figure reproduced from [2].

the remainder of the impeller, not in the inducer. A purpose of the inducer is to ensure smooth flow to enter the rest of the impeller. We will in the following determine a condition for which boundary layer separation is prevented on the inducer surface. Moreover, we will calculate the maximal rotational speed of the shaft. This will give useful information on different design specifications of the compressor. Figure 9 displays velocity triangles at the root, mean and tip radii. Here, *tip* refers to the inlet tip of the impeller. The angle between the relative velocity vector and the flow at the impeller tip can be very large. The vane near the tip must therefore be set at an angle large with respect to the axial direction. This ensures the flow to enter the inducer without any leading-edge separation. Because separation can occur on the curved inducer surface, there is a limit to the amount of turning that can be produced in the inducer.

We may assume that the inducer achieves the turning of the relative velocity vector without any change in radius. The velocities in a cylindrical section of radius r_1 are shown in Figure 9. With no radial velocity component in the inducer, continuity for incompressible flow requires a constant axial velocity component. The relative velocity at the inducer outlet is therefore

$$w'_t = w_{1t} \cos \beta_{1t}. \quad (44)$$

Having $w' < w_1$ implies diffusion in the inducer. Next, we define a pressure coefficient

$$C_p = \frac{p' - p_1}{\frac{1}{2} \rho w_1^2} = 1 - \left(\frac{w'}{w_1} \right)^2, \quad (45)$$

in which p' is the static inducer outlet pressure. The maximum allowed turning angle that does not produce separation on the inducer surface is therefore

$$\cos \beta_1 = \sqrt{1 - C_{p,\max}}. \quad (46)$$

For turbulent boundary layers, choosing $C_{p,\max} = 0.6$ gives a maximum turning angle of around 50° . However, the separation may happen earlier on a curved surface than on a flat one, having the same variation in pressure with distance in the flow direction. Compressibility in the inducer can also lead to shocks at high Mach numbers. To avoid shocks it has previously been suggested that supersonic velocities must be prevented. More modern

methods of flow analysis have instead helped developed transonic flow designs, implying both subsonic and supersonic flow along the impeller.

We will now determine the maximal rotational speed of the shaft by restricting the maximal Mach number of the entering flow, as well as restricting the inlet tip blade angle. This allows us to plot the rotational speed as a function of absolute Mach number M_1 of the entering flow and determine the minimum size of the rotor. First we find the inlet relative Mach number to be

$$M_{1\text{ rel}} = M_1 / \cos \beta_{1t}. \quad (47)$$

Next, we need the inlet temperature T_1 , density ρ_1 and velocity c_1 , which are

$$T_1 = T_{01} \left/ \left(1 + \frac{\gamma - 1}{2} M_1^2 \right) \right., \quad (48)$$

$$\rho_1 = \rho_{01} \left/ \left(1 + \frac{\gamma - 1}{2} M_1^2 \right)^{1/(\gamma-1)} \right., \quad (49)$$

$$c_1 = M_1 \sqrt{\gamma R T_1}. \quad (50)$$

The blade-tip velocity at the inducer inlet plane reads

$$U_{1t} = c_1 \tan \beta_{1t}, \quad (51)$$

while the inlet tip diameter is

$$D_{1t} = \sqrt{D_h^2 + \frac{4}{\pi} \frac{\dot{m}}{\rho_1 c_1}}, \quad (52)$$

where D_h is the hub diameter and $4\dot{m}/\pi\rho_1 c_1$ is the square of the diameter necessary for a mass flow \dot{m} . By combining these expression, we find the shaft speed (rpm) to be

$$N = \frac{60}{\pi} \frac{U_{1t}}{D_{1t}}. \quad (53)$$

The relation between absolute and relative axial mach number to shaft speed, as well as the dependency on inlet tip blade angle are shown in Figure 10. The numerical values are obtained for hydrogen gas with $D_h = 0.1$ m, $T_{01} = 300$ K, $p_{01} = 1$ bar and a flow rate of 30 kg/s. As an example, keeping $\beta_{1t} < 50^\circ$ to avoid separation at the inducer surface and $M_{1\text{ rel}} < 1.4$ gives a maximum shaft speed of 6000 rpm. The exit tip speed is usually set by the required pressure ratio of the stage. Hence, the maximum shaft speed calculated here fixes the minimum size of the rotor. Essential design limitations of centrifugal compressors are therefore:

1. Aerodynamics where inlet relative Mach number at the tip limits the rotational speed
2. Material stress which limits the impeller tip speed.

4.6 Flow separation at impeller exit

To reduce the chance of boundary layer separation, it is beneficial to keep the average flow velocity roughly constant in the radial flow part of the impeller. This can be achieved by decreasing the axial width of the impeller passage with increasing radius. In a stationary diffuser, pressure is rising because of the fluid being slowed down. However, this is not the case in the impeller where pressure is rising rapidly in the flow direction

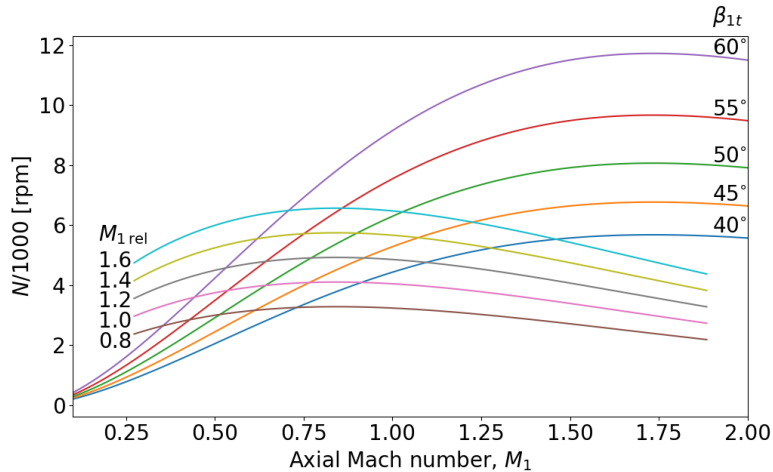


Figure 10: Rotational speed (rpm) of a centrifugal hydrogen compressor inducer when $\dot{m} = 30 \text{ kg/s}$, $D_h = 0.1 \text{ m}$, $p_{01} = 100 \text{ kPa}$ and $T_{01} = 300 \text{ K}$.

due to centrifugal forces, and not boundary layer separation. Schumann, Clark and Wood studied how pressure and velocity distributions were affected by rotor passage velocity ratio w_2/w_1 , in which w_2 and w_1 are the passage average relative velocities at outlet and inlet of the rotor [3]. To do so they reduced the exit blade height of the rotor in a series of steps. They showed that flow passage separation would arise if w_2/w_1 dropped below a certain value (~ 0.7 for air). Therefore, flow passages in centrifugal rotors act like nonrotating diffusers since they give rise to flow separation at a certain overall velocity ratio. The same happens in axial compressor rotors. As deceleration in the inducer is inevitable and must be kept to a minimum of around 0.7 for air, the mean relative velocity in the rest of the flow passage should be kept nearly constant. Controlling the mean velocity w limits the inlet to outlet variation in blade width.

We will now examine how the Coriolis forces behave in the impeller as this gives rise to a pressure gradient in the tangential direction. In Figure 11, a particle of fluid travels radially outward at a velocity w relative to the impeller. The rotational velocity is Ω . The absolute and relative velocities of the particle, c and w , at time t are shown in full lines. The broken lines depict the absolute and relative velocities, c' and w' , at time $t + dt$. At this time, the magnitude of the relative velocity is unchanged, but the absolute velocity has changed. For infinitesimal dt and $d\theta = \Omega dt$, we find that $dc_\theta = \Omega dr + wd\theta$ which corresponds to the change in θ -direction. This can be rewritten to

$$dc_\theta = \Omega w dt + w \Omega dt. \quad (54)$$

The Coriolis acceleration $a_\theta = dc_\theta/dt$ is therefore

$$a_\theta = 2\Omega w, \quad (55)$$

with the resulting pressure gradient in the tangential direction having magnitude

$$\frac{1}{r} \frac{\partial p}{\partial \theta} = -2\rho\Omega w. \quad (56)$$

The tangential pressure gradient gives rise to a positive gradient of w in the tangential direction. Using Eq. (25) in the tangential direction we can determine its magnitude by writing

$$\frac{1}{\rho} \frac{dp}{rd\theta} = -\frac{d\left(\frac{w^2}{2}\right)}{rd\theta} = -\frac{w}{r} \frac{dw}{d\theta}, \quad (57)$$

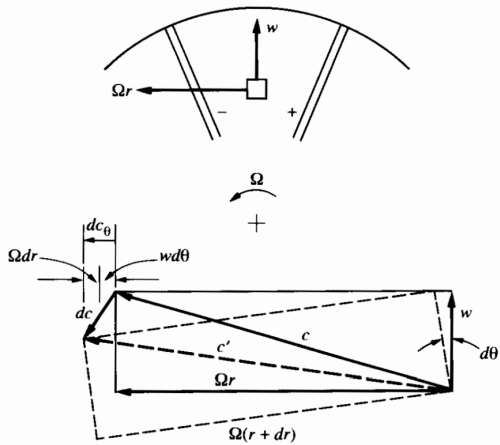


Figure 11: Coriolis acceleration in a centrifugal impeller. Figure reproduced from [2].

in which we assume all streamlines to have the same pressure in the rotating frame of reference. Together with Eq. (56), we find that

$$\frac{1}{r} \frac{dw}{d\theta} = 2\Omega. \quad (58)$$

Hence, the tangential variation in relative velocity is independent of flow rate.

The Coriolis pressure gradient gives rise to a pressure difference across the blades, with higher pressure on the leading face of the blades. However, at the exit of the impeller we will have an almost constant static pressure in the tangential direction. Hence, near the tip of the impeller the flow will undergo adjustments with three consequences:

1. A fluid particle in the middle of the channel will not be able to continue in a purely radial direction as the Coriolis pressure is reduced and disappears toward the impeller exit. The particle will therefore slip back against the direction of rotation. As a result, the absolute tangential velocity $c_{\theta 2}$ will be considerably less than U_2 . This effect increases the required work and becomes stronger for a small number of blades. Inserting extra blades that reaches only part way to the hub can thus be an option.
2. On the high pressure side of the blade, the fluid will be accelerated as the pressure drops towards the exit. This tends to keep the boundary layer on the outer part of the pressure surface well behaved.
3. On the low pressure/suction side of the blade, the opposite will happen. Here, the pressure gradient becomes even more negative as one approaches the impeller exit. This tends to cause boundary layer separation. The dynamics happening on this side is complex and may be hard to predict accurately. Because of flow separation on the suction side, several designs show backward-tipped blades, even though this can increase bending stress.

Potential flow calculations have been used to study the effect of blade spacing and exit angle on the ratio $c_{\theta 2}/U_2$. We start out by defining a slip factor

$$\sigma_s = \frac{c_{\theta 2}}{U_2}, \quad (59)$$



SINTEF

where $c_{\theta 2}$ is the momentum-averaged tangential velocity component. Stanitz showed that the slip factor for an impeller with more than 10 radial blades is

$$\sigma_s \approx 1 - \frac{2}{N_b}, \quad (60)$$

in which N_b is the number of blades. Back-swept blades modifies the slip factor to

$$\sigma_s = \left(1 - \frac{2}{N_b \sqrt{\cos B_2}}\right) \left(1 - \frac{w_{r2}}{U_2} \tan B_2\right), \quad (61)$$

where B_2 is the exit blade angle with respect to the radial direction. This agrees with Eq. (60) in the limiting case of straight radial blades with $B_2 = 0$. Furthermore, we rewrite this in terms of β_2 as

$$\tan \beta_2 = \tan B_2 + \frac{2}{N_b} \sqrt{\cos B_2} \left[1 / \left(\frac{w_{r2}}{U_2} \right) - \tan B_2 \right], \quad (62)$$

in which we know that β_2 , U_2 and $c_{\theta 2}$ are related as $w_{r2} \tan \beta_2 = U_2 - c_{\theta 2}$. Note that β_2 is related to the outlet relative velocities, while B_2 describes the positioning of the blades. If $w_{r2} \rightarrow 0$, we observe that $\beta_2 \rightarrow 90^\circ$ for all values of B_2 .

4.7 The diffuser

The fluid will leave the impeller with a high absolute velocity. This velocity is decreased in the diffuser in order to increase the pressure. The diffuser can consist of a vaneless region and a region with vanes as illustrated in Figure 12. First, we examine what takes place in the vaneless region, $r_1 < r < r_2$. From continuity it follows that an incompressible flow in a vaneless region of constant axial width h satisfies

$$\dot{m} = \rho(2\pi rh)c_r = \text{constant} \quad \text{or} \quad rc_r = \text{constant}. \quad (63)$$

Neglecting wall friction, we know that angular momentum must be conserved throughout the vaneless region, meaning $rc_\theta = \text{constant}$. Together with Eq. (63) we find

$$\frac{c_\theta}{c_r} = \text{constant} = \tan \alpha, \quad (64)$$

where we have defined α as the angle between the velocity and the radial direction. Streamlines will therefore follow a logarithmic spiral in which they make a constant angle with the radial direction. Moreover, because α is constant we observe that velocity is inversely proportional to radius, $c_2/c_1 = r_1/r_2$.

On the other hand, we can examine compressible flow by assuming reversible flow. We start out by relating the fluid properties at any point to a point with unity Mach number. Conservation of angular momentum requires that

$$\begin{aligned} \rho r c \cos \alpha &= \rho^* r^* c^* \cos \alpha^*, \\ rc \sin \alpha &= r^* c^* \sin \alpha^*, \end{aligned} \quad (65)$$

where $*$ denotes the value reached in reversible adiabatic flow from the local condition until the Mach number is 1. Combining the equations, we are left with

$$\frac{\tan \alpha^*}{\tan \alpha} = \frac{\rho^*}{\rho} = \left[\frac{2}{\gamma + 1} \left(1 + \frac{\gamma - 1}{2} M^2 \right) \right]^{1/(\gamma-1)}, \quad (66)$$

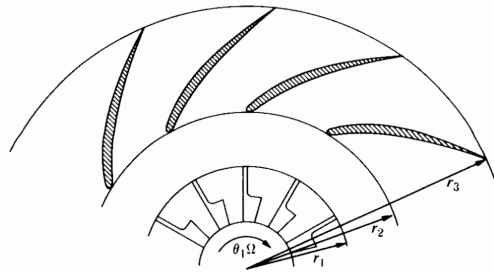


Figure 12: Radial diffuser with a vaneless region and a region with vanes. Figure reproduced from [2]

where we have made use of Eq. (49). Together with Eq. (65), we find a relation between r and M that reads

$$\frac{r^* \sin \alpha^*}{r \sin \alpha} = \frac{c}{c^*} = M \sqrt{T/T^*}. \quad (67)$$

The isentropic equation (48) then yields

$$\frac{r^* \sin \alpha^*}{r \sin \alpha} = M \left\{ \frac{(\gamma + 1)/2}{1 + [(\gamma - 1)/2] M^2} \right\}^{1/2}. \quad (68)$$

The * quantities are found from known inlet conditions. This allows us to determine the angle α from Eq. (67) and r from Eq. (68), as a function of M .

For a given γ , we can determine the radius ratio r_2/r_1 of the diffuser. First, we use the known angle, α_1 , and Mach number, M_1 , to find $(r/r^*)_1$ and α_1^* . The state of the fluid will follow a line of constant α^* until a desired Mach number, M_2 , is achieved. As a result, the radius ratio of the diffuser becomes

$$\frac{r_2}{r_1} = \frac{(r/r^*)_2}{(r/r^*)_1}. \quad (69)$$

A line having constant α^* can either correspond to supersonic acceleration or diffusion. However, only the latter is relevant for compressors. Vaneless diffusers are beneficial because they can provide deceleration from supersonic to subsonic flow without causing shocks. However, to demonstrate the need for a region of vanes, we choose as an example $M_1 = 1.3$ and $\alpha_1 = 70^\circ$. Hence, $\alpha^* = 75^\circ$ and $(r/r^*)_1 = 0.8$. A diffusion where the Mach number reaches $M_2 = 0.4$ gives $(r/r^*)_2 = 2.3$, which in turn yields

$$\frac{r_2}{r_1} = \frac{2.3}{0.8} = 2.9. \quad (70)$$

Having only a vaneless diffuser can therefore lead to a very large diameter. A following region with vanes can consequently be helpful to increase pressure more rapidly in the radial direction.



5 Total work and compression ratio for hydrogen

In this chapter, we will establish how the total work of a compressor can be calculated for a given pressure ratio. This, in contrast to calculating the work from e.g. the stagnation enthalpy rise as done in section 4.2. Thereby, we can compare the work necessary to compress hydrogen and methane. Calculating the required work to compress a gas needs the knowledge of an appropriate equation of state and a calorific equation. This is not widely available for hydrogen [4]. We will therefore show how the work can be calculated by assuming either an isentropic, isothermal or so-called polytropic compression.

An often used approach is to assume the compression of hydrogen to be an isentropic (adiabatic) process. In other words we consider a reversible process where there is no heat exchange between the compressor and the environment. Adiabatic conditions imply that pV^γ is a constant and isentropic conditions $\Delta S = 0$ means that the process is reversible. The work required to increase the pressure of a gas p is

$$W = \int_{V_1}^{V_2} p dV, \quad (71)$$

where V is the volume of the gas. For an ideal gas, the isentropic (adiabatic) work to compress 1 mole (or 2.02 g of hydrogen) from a pressure p_1 to a pressure $p_2 > p_1$ is

$$W_{\Delta S \rightarrow 0, \text{ideal}} = \frac{\gamma}{\gamma - 1} R T_1 \left[\left(\frac{p_2}{p_1} \right)^{\frac{\gamma-1}{\gamma}} - 1 \right], \quad (72)$$

where T_1 is the temperature at p_1 . The specific heat ratio $\gamma = C_p/C_V = 1.4$ for all diatomic gases like hydrogen and the universal gas constant $R = 8.314 \text{ J/K mol}$. Figure 13 displays the necessary isentropic work in order to compress hydrogen and methane, assuming ideal gas behaviour, from an inlet pressure of $p_1 = 1 \text{ bar}$ up to a given discharge pressure p_2 for a single stage compressor. As expected, hydrogen requires significantly more work to reach a given discharge pressure compared to methane. Deviation from the ideal reversible process is

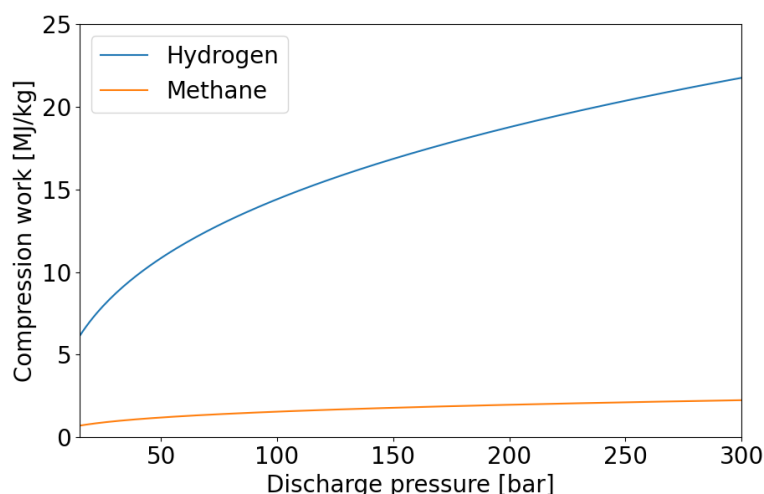


Figure 13: Isentropic work required to compress hydrogen and methane, assuming ideal gas behaviour, from an inlet pressure of 15 bar up to a given discharge pressure for a single stage compressor.

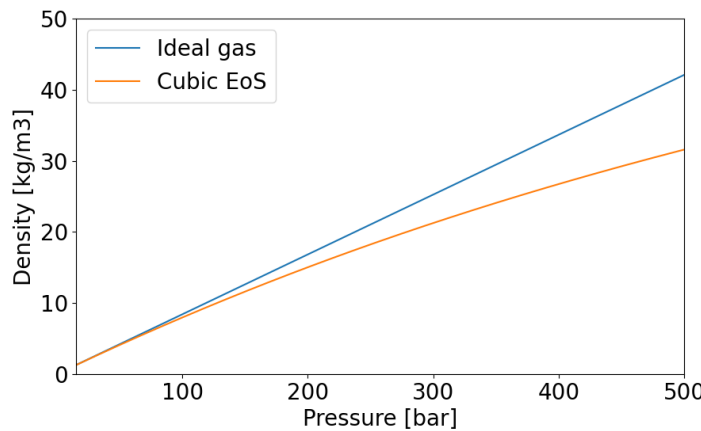


Figure 14: Density of hydrogen gas as a function of pressure at $T = 15^\circ\text{C}$.

accounted for by introducing an isentropic compressor efficiency. The actual work is then given by

$$W_{\text{actual}} = \frac{W_{\Delta S \rightarrow 0, \text{ideal}}}{\eta_{\text{adiabatic}}} . \quad (73)$$

The adiabatic efficiency $\eta_{\text{adiabatic}}$ is typically of the order of 75–85 % [4]. Finally, the electrical consumption of the compressor can be found by taking into account the efficiency of the electrical motor, which is typically of the order of 90 %. However, assuming that hydrogen behaves as an ideal gas can give rise to significant errors at higher pressures, although pressures below 100–150 bar may not be problematic as illustrated in Figure 14 for the density of hydrogen.

The required work of compression for one mole can also be computed assuming an isothermal process, using different ideal and real gas models:

(a) for an ideal gas:

$$W_{\text{isothermal, ideal}} = RT \ln \frac{V_1}{V_2}$$

(b) for a van der Waals gas:

$$W_{\text{isothermal, Walls}} = RT \ln \frac{V_1 - b}{V_2 - b} - \frac{\alpha}{V_2} + \frac{\alpha}{V_1} \quad (74)$$

(c) for a compressible gas (Z-factor):

$$W_{\text{isothermal, Z}} = ZRT \ln \frac{V_1}{V_2} ,$$

Herein, the empirical constants in the van der Waals gas model are $\alpha = 0.0244 \text{ Pa}(\text{m}^3)^2\text{mole}^{-2}$ and $b = 0.0266 \cdot 10^{-3} \text{ m}^3\text{mole}^{-1}$. The empirically determined compressibility factor Z represents the deviation of a real gas from an ideal gas, and depends on the pressure, temperature and substance. An isothermal process is characterized by having $pV = \text{constant}$. The choice of gas model can greatly affect the calculated required work for an isothermal compression.

The actual form of the compression will generally be between an isothermal and isentropic compression. The former represents a lower limit of the compression work, while the latter represents an upper limit. A polytropic process where pV^n is constant can better approximate the compression process. The polytropic

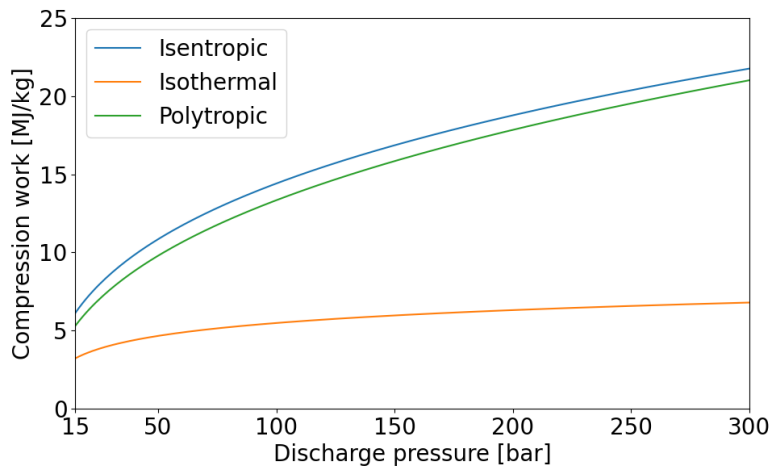


Figure 15: Work required to compress hydrogen, assuming ideal gas behaviour, from an inlet pressure of 15 bar up to a given discharge pressure for a single stage compressor. Plotted for an isentropic, isothermal and polytropic compression process. Adiabatic efficiency $\eta_{\text{adiabatic}} = 0.8$ and polytropic efficiency $\eta_p = 0.85$.

index n is dependent on the details of the compression process and the nature of the gas. For $n > \gamma$, heat is injected into the gas during compression. For $n < \gamma$, heat is rejected by the gas during compression. Substituting n for γ in Eq. (72) for the required adiabatic work yields the performed work during a polytropic compression:

$$W_{\text{polytropic}} = \frac{n}{n-1} RT_1 \left[\left(\frac{p_2}{p_1} \right)^{\frac{n-1}{n}} - 1 \right]. \quad (75)$$

The actual required compression work will also here be larger than the work calculated in Eq. (75). Knowing the polytropic efficiency η_p , we can relate the polytropic index to the specific heat ratio:

$$n = \frac{\eta_p \gamma}{1 + \eta_p \gamma - \gamma} \quad \text{and} \quad \frac{n}{n-1} = \frac{\gamma}{\gamma-1} \eta_p. \quad (76)$$

The polytropic efficiency is often given by the equipment manufacturers. Figure 15 shows the work required to compress hydrogen for an isentropic, isothermal and polytropic process. A polytropic process will change the gas temperature from T_1 to

$$T_2 = T_1 \left(\frac{p_2}{p_1} \right)^{\frac{n-1}{n}}. \quad (77)$$

We observe that temperature increases with final pressure. Moreover, Figure 15 shows that an isothermal process, where temperature is kept constant, is favorable. Cooling during the compression process can therefore reduce the required work. Cooling while compressing is impractical. Another strategy is therefore to use a multi-stage compressor with cooling between the stages, i.e. intercooling. With perfect intercooling, where the temperature is reduced to the initial temperature, the isentropic work of a two-stage compressor becomes

$$W_{\Delta S \rightarrow 0} = \frac{\gamma RT_1}{\gamma-1} \left[\left(\frac{p_2}{p_1} \right)^{\frac{\gamma-1}{\gamma}} - 1 \right] + \frac{\gamma RT_1}{\gamma-1} \left[\left(\frac{p_3}{p_2} \right)^{\frac{\gamma-1}{\gamma}} - 1 \right], \quad (78)$$

in which p_1 and p_3 are the initial and discharge pressures. The optimal intermediate pressure $p_2 = \sqrt{p_1 p_3}$. This ensures the same pressure ratio in each compression stage which is a condition for minimal work. Increasing

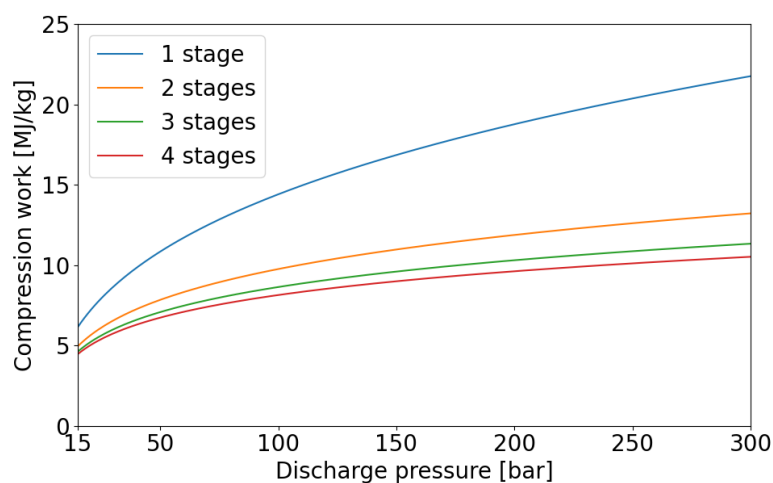


Figure 16: Isentropic work required to compress hydrogen, assuming ideal gas behaviour, from an inlet pressure of 15 bar up to a given discharge pressure. Plotted for varying number of compressor stages with an adiabatic efficiency $\eta_{\text{adiabatic}} = 0.8$ and ideal stage intercooling.

the number of stages will reduce the work, but adding numerous stages may not result in any substantial energy efficiency gain. This can be seen in Figure 16 where the relation between compression work and discharge pressure is plotted for an increasing number of stages. On the contrary, 2 or 3 stages may not be sufficient to deliver a high discharge pressure since the pressure ratio of each stage will be limited. It can be noted that for a discharge pressure of 800 bar (far higher than needed in hydrogen pipelines), the compressive energy requirement of a multi-stage centrifugal compressor is approximately 12 % of the hydrogen energy content [1]. Independent of the compression process, the relation between compression work and discharge pressure is parabolic and not linear. Increasing the pressure from 150 to 200 bar is therefore easier than increasing it from 50 to 100 bar. Hence, having a high inlet pressure is favorable. The required number of stages to reach a discharge pressure of 100 bar has been calculated for different inlet pressures in [5]. Here, they use a set isentropic efficiency.



6 Hydrogen compression - State of the art

Pipeline transportation over long distances appears to be the most economical way of transporting hydrogen. It requires less energy per unit than trucks as well as being safer [1]. A new hydrogen pipeline network can be built parallel to the existing natural gas grid or the existing grid can be converted into transporting hydrogen [6]. Either way, one has to select the appropriate pressure upstream of the pipeline. This is dependent on flow velocity, ambient temperature, thermal insulation layer, and the geometric characteristics of the pipeline, such as diameter, length, and elevation changes. The existing natural gas pipelines are operated at relatively low pressure levels, typically around 20–30 bar. For hydrogen, some of the new pipelines are designed to operate at pressures up to 100 bar [1]. Others propose up to 200 bar. Although hydrogen is very heavy (about three times that of gasoline) and has a high gravitational energy density, it has a very low volumetric energy density due to the low molar weight. At standard conditions, the volumetric energy of natural gas is 36.4 MJ/m³, while the volumetric energy of hydrogen is 10.05 MJ/m³. At 200 bar and 15 °C, natural gas has a volumetric energy of 6860 MJ/m³ while it is 1825 MJ/m³ for hydrogen [1]. This explains the high pressures needed for hydrogen and implies that hydrogen compression is a pressing challenge that needs to be tackled.

In this section, we start out by reviewing the state of gas pipelines and compressor stations today. In addition, we mention the typical pressures at which hydrogen is produced. This may be equal to the input pressure of the pipeline compressors and is an important parameter deciding the compressor complexity and required compressor work. Next, we assess hydrogen compression for discharge pressures up to 100 bar and mass flows around 10–21 t/h. Next, we assess the possibility of hydrogen compression for discharge pressures up to 200 bar and mass flows around 300 t/h. The latter has more relevance to Norwegian pipeline export, but is minimally discussed in the literature.

6.1 General requirements and inlet pressure

In 2020, the worldwide production of hydrogen was about 120 Mt/a. This is expected to rise to 530 Mt/a by 2050 [5]. The diameter of the existing European transmission gas pipelines is typically between 400 and 1400 mm. They operate at pressures ranging from 16 to 100 barg [7]. The flow velocity ranges between 10 and 20 m/s depending on the pipeline design [5]. Typically, valves are placed with a spacing of 8–30 km [7]. A recompression of the pressurized gas is necessary because of pressure loss in the pipeline system, and is carried out every 100 to 600 km. Unlike the pipeline sections, existing centrifugal compressors used for natural gas cannot be repurposed for pure hydrogen since impeller tip speeds might have to be tripled because of the low molecular weight of hydrogen.

Although regulations for hydrogen production, handling, compression and export are still in development, the NORSO standards give important information. NORSO standards are developed by the Norwegian petroleum industry and published by Standards Norway [8]. The standards are prepared to ensure safety, value adding and cost effectiveness. They present a rule of thumb for the maximal gas velocity in pipelines when pressure drop is not critical, i.e. when further pressure drop will still result in increased gas velocity. To avoid noise or vibration problems, they state that gas velocity should be kept below

$$v = \min \left(175 \left(\frac{1}{\rho} \right)^{0.43}, 60 \text{ m/s} \right), \quad (79)$$

where v is the velocity in m/s and ρ is the density of gas in kg/m³.

Generally, compressing a gas increases its temperature. To allow high discharge temperatures, centrifugal compressors may be designed with high-temperature O-rings and center-supported diaphragms. In [9], they



SINTEF

suggest using foil bearings for high-speed centrifugal compressors. As mentioned, when designing compressors for gases of higher molecular weight, the material strength limitations are usually not an issue since the Mach numbers will instead limit the operating speed. However, the speed of sound in lighter gases like hydrogen is far higher, causing material strength limitations to be an issue because of the required high speed of the impellers. For instance, to achieve the same pressure ratio in hydrogen as air requires the impeller tip speed to increase by a factor of 3.8, resulting in a stress increase in the rotor by a factor of $3.8^2 = 14.4$ [10]. Additionally, this is complicated by the potential hydrogen embrittlement, i.e. hydrogen-induced cracking of the material.

Having a high inlet pressure to the compressor can reduce both the complexity of the compressor and required compressor work as shown in chapter 5. The inlet pressure will depend on the output pressure of the produced hydrogen. Hydrogen can be produced as green hydrogen from electrolysis where the output pressure will be relatively low. Output pressure from electrolyzers using alkaline technology ranges from ambient to 25 bar, while it is around 35 bar for PEM electrolysis. A couple of examples include [11]:

- Alkaline: Hydrogenics HySTAT™ 15–25 barg, Etogas 15 bar, Tractebel 0–15 bar.
- PEM: Siemens Silyzer 200/300 35 bar, Tractebel 30–60 bar. Due to technological innovation, it is expected that this may increase towards 60 barg.

Alternatively, one can produce blue hydrogen from natural gas with carbon capture and storage (CCS). The latter can provide higher compressor inlet pressure and larger mass flow rates. Due to material properties and operating costs, large amounts of gaseous hydrogen are usually not stored at pressures of more than 100 bar in ground tanks and 200 bar in underground storage [1].

6.2 Medium scale compression

Compression of hydrogen to 100 bar has been discussed in the literature. Although this is lower than what is proposed for Norwegian export, we will describe some of the recent developments. The flow rates associated with these pressures are typically also smaller than what is relevant to Norwegian export. In [12], they analyze hydrogen compression and pipeline transportation over 50 km and a pressure of 100 bar upstream a pipeline. They propose the following for different flow rates:

- Flow rates of 0.7–1.8 t/h: three-stage reciprocating compressor.
- Flow rates of 3.6–7.2 t/h: compression train made up of a conventional, two-section multi-stage centrifugal compressor followed by a two-stage reciprocating compressor.
- Flow rate of 10 t/h: an advanced eight-stage, integrally geared centrifugal compressor operating at a blade tip speed near 600 m/s.

In [1], they estimate that a large scale hydrogen production plant has an output of around 200 000 Nm³/h (normal volume per hour) or 21 t/h at standard conditions. In the same review article, they present a comparison of different hydrogen compression technologies for different mass flow rates and discharge pressures. Even though 21 t/h may be less than what is needed for Norwegian export, it is seen that the only relevant compression technologies are reciprocating compressors and, in particular, centrifugal compressors. Typical application ranges for reciprocating and centrifugal compressors are also displayed in [1]. In general, centrifugal compressors can handle larger flow rates while reciprocating compressors can potentially achieve higher discharge pressures. However, reciprocating compressors are limited by difficult maintenance. The minimal and maximal capacities of centrifugal compressors are limited by choking and surging, respectively. As a side note, a typical turn down ratio (ratio of maximum capacity to minimum capacity) for constant speed multi-stage



SINTEF

centrifugal compressors is about 20–30 %. The ratio can be increased to 40–50 % by altering the speed or adding adjustable inlet guide vanes [1].

In [1], they claim that pressure ratios for hydrogen is limited to 1.05–1.2 in a single compression stage. Using high-strength titanium alloys together with proper design of the blades and impeller geometry, they show in [10] that pressure ratios of up to 1.35 per stage can be achieved for hydrogen. Moreover, they illustrate the relationship between overall pressure ratio, impeller tip speed and material stress. For high impeller speeds one is dependent on impellers made of advanced composites, while at lower speeds, high strength alloys are sufficient. The same technical report claim that they have built machines with tip speeds of up to 700 m/s together with hydrogen pressure ratios of a single stage of over 1.45. Hence, it is concluded that a six-stage compressor with total pressure ratio of 4 is technically possible.

6.2.1 Six-stage centrifugal hydrogen compressor

The main part of the above mentioned technical report describes the design and construction of a six-stage centrifugal hydrogen compressor in accordance with the following objectives put forward by the US Department of Energy (DOE) [10]:

- Delivery of 4 to 40 t/h of 99.99 % hydrogen gas from generation site(s) to forecourt stations.
- Compress hydrogen from 350 psig (24 bar) to 1000 psig (69 bar) or greater.
- Reduce initial installed system equipment cost.
- Reduce package footprint and improve packaging design.
- Achieve transport delivery costs to below \$1/GGE (gasoline gallon equivalent).
- Reduce maintenance cost to below 3 % of Total Capital Investment by fiscal year 2017.
- Increase system reliability to avoid purchasing redundant systems.
- Maintain hydrogen efficiency (as defined by DOE) to 98 % or greater.
- Reduce H₂ leakage to less than 0.5 % by fiscal year 2017.

The project successfully finalized the design of a six-stage centrifugal compressor, fulfilling the above DOE engineering specifications. They also manufactured and successfully tested a single stage of the compressor. Testing the full six-stage compressor has been delayed until additional funds are obtained. Different features of the compressor are:

- Overall pressure ratio of 3.56.
- Each stage provides a pressure ratio of 1.26.
- Designed to compress 10 t/h of hydrogen from 24 bar to 89 bar.
- Each stage has the same aluminum impeller with a diameter of 203 mm.
- All stages are integrally driven by a single-step gearbox. The integral gearbox pinions drives individual overhung impellers. Overhung impellers are installed on a shaft that is suspended at *one* end by bearings. This is opposite to between bearing where one or several impellers are installed on a shaft that is suspended at *both* ends between two bearings.



SINTEF

- The electric motor drive is a 1800-rpm synchronous electric motor rated at 6600 kWe.
- Nominal shaft speed of 60000 rpm.
- Intercooling between each stage, maintaining a maximum stage discharge temperature of less than 66 °C.
- Low temperature enabled the use of an aluminum alloy compatible with hydrogen and structural robust enough to operate at a tip speed of 640 m/s.
- The inlet to the compressor volute (diffuser) included a low-solidity airfoil in order to improve diffuser performance, and thus, the overall efficiency of each stage.
- Designed with commercially available components.
- Total selling price estimated in 2015 was USD 3 625 000, where 40 % constitutes material costs.

The predicted compressor performance map of the six-stage compressor is found in [10]. Several compressor performance maps accounting for emergency shutdown can also be found in [10] on page 71 and onwards. It can be noted that a more advanced, experimental compressor rotor design was reviewed for the same overall pressure ratio, but with five stages instead of six. This approach was abandoned since the power per stage was slightly higher than could be supported by commercially available bearings. Other configurations of the hydrogen compressor were also considered. The energy efficiency as a function of pressure ratio for alternative designs of the compressor is shown in [10]. It is important to be aware that even though vendors report a high maximal pressure ratio, one should avoid operating in this regime as this may wear out different parts of the compressor leading to high maintenance requirements.

6.2.2 Eight-stage centrifugal hydrogen compressor concept

A concept for an eight-stage integrally geared hydrogen compressor with an inlet pressure of 20 bar and final pressure of 80 bar has been presented in [12]. The flow rate is adjusted to 10 t/h. Moreover, the blade tip speed is almost 600 m/s. The thermodynamic path of the compression process is presented in Figure 17. It is assumed that intercooling reduces the hydrogen temperature to 40 °C between each stage without any pressure loss. A diagram of the compressor concept and a sketch of the structural features are shown in [12].

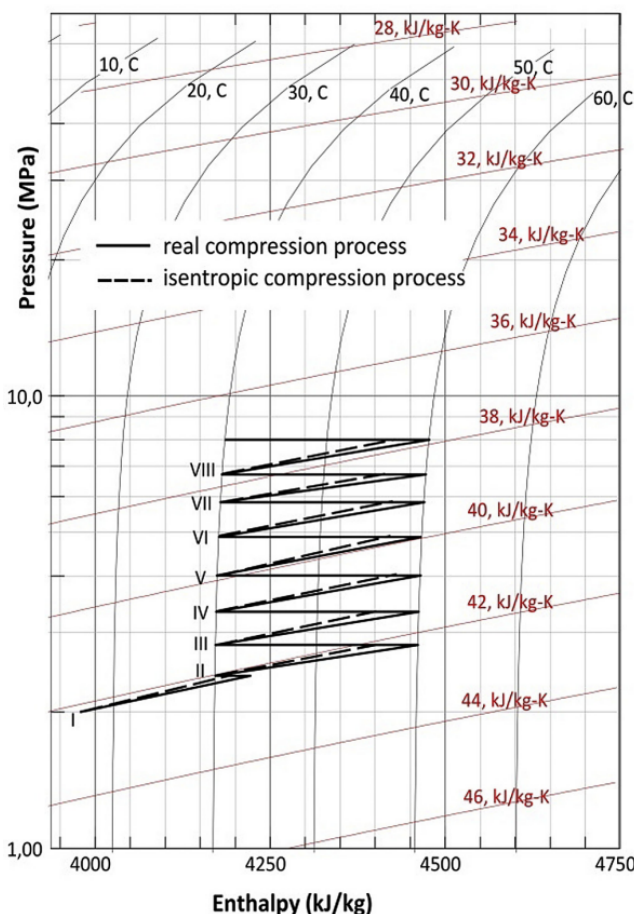


Figure 17: The thermodynamic path of an eight-stage integrally geared centrifugal hydrogen compressor concept. Figure reprinted from [12] with permission from Elsevier.

6.3 Large scale compression

Export of hydrogen from Norway to continental Europe requires long pipelines which in turn requires high pressures due to pressure loss in the pipeline system. A compressor discharge pressure of up to 200 bar may therefore be necessary. Moreover, mass flows up to 300 t/h may also be assessed. In 2022 the BarMar project was announced which aims at transporting hydrogen from Barcelona to Marseille. The 455 km long pipelines will operate at a pressure of 210 bar, having a diameter of 28 inches and maximum transmission capacity of 2 million tonnes per annum (= 228 t/h). Maximum depth below sea level for the pipelines is 2600 m. The compressor station will have a power of 140 MW in a 3+1 configuration. A budget of 2.5 billion euros is estimated for the project as a whole.

There exists a number of compressors that can deliver hydrogen at 210 bar. At the same time, allowing for a flow rate in the range 200–300 t/h might also be possible with existing reciprocating compressor, but will lead to high maintenance requirements. The resulting operational expenses may therefore be regarded as too high. As a consequence, centrifugal compressor can become the solution. In the open literature it has not been possible to find any detailed examples of centrifugal compressors that can deliver such high discharge pressures and flow rates.



SINTEF

7 Hydrogen admixture to natural gas

An alternative to compressing and transporting pure hydrogen is to blend hydrogen into natural gas. In that case it is interesting to see if existing centrifugal compressors can be utilized. In [13] page 16 they discuss two studies which addresses the required impeller speed for increasing hydrogen admixture. Both studies model centrifugal compressors with off-design performance maps. In a scenario with constant volumetric flow rate, the impeller speed changes minimally when a composition of up to 20 % hydrogen by volume is considered. However, for a constant energy throughput scenario, impeller speed must increase considerably for natural gas mixtures with only 10 % hydrogen. The speed of these existing compressors will exceed safe operating limits based on the API standard 617, where maximum operating speed is set to 105 % of design speed.

Another option is to replace the impeller and other compressor internals with components designed for greater hydrogen compositions. This might be a cheaper alternative compared to a complete replacement of the compressor. It can be noted that API standard 617 prohibits the use of steel materials with yield strengths greater than 827 MPa or hardness in excess of Rockwell C 34 for centrifugal compressors, in which the hydrogen partial pressures are greater than 6.89 bar. This also applies to centrifugal compressors where the hydrogen concentration exceeds 90 molar percent at any pressure. A concern is blistering, where hydrogen diffuses through the material and induces local pressure buildup at inclusions or grain boundaries. This can produce crack propagation.



SINTEF

8 Compressor performance code

Centrifugal compressor performance (ccp) is a Python library for calculation of centrifugal compressor performance with gas as the working fluid [14]. It allows you to construct a compressor with multiple performance points (suction state, discharge state, volume flow, etc.) and calculate different characteristics of the compressor such as efficiency, head and power. Factory performance testing following the ASME PTC 10 standard is also possible. The code runs fast and is an alternative to running lengthy CFD simulations. A quick tutorial is found at https://ccp-centrifugal-compressor-performance.readthedocs.io/en/latest/user_guide/tutorial.html. The code originally uses CoolProp [15] and REFPROP [16] for the gas properties calculations. However, we have replaced these libraries with open-source libraries, called Thermopack and Thermphys [17], both having a Python interface. Thermopack is a thermodynamics library for multi-component and multi-phase thermodynamics developed at SINTEF Energy Research and NTNU Department of Chemistry. In ccp, Thermopack is used for all gas properties calculations, except the calculation of viscosity and thermal conductivity, which is performed by Thermphys. Thermphys is also developed at SINTEF Energy Research. Tests have been performed in order to validate the new version using Thermopack and Thermphys against the previous version using CoolProp and REFPROP.

In the following, we will give an outline of the different modules of the ccp code and how these run. For each module we have created example code that how to define

8.1 Working principles

The ccp code contains five main modules with corresponding Python classes: State, Point, Curve, Impeller and Compressor. A flow diagram depicting the relation between these classes is shown in Figure 18. The code can be utilized on different levels. For instance, we can define a single impeller and calculate performance characteristics of the impeller alone. Alternatively, we can calculate the same characteristics of a full compressor. At the moment, it is only possible to define a straight-through compressor with one section or a compressor with two sections in a back-to-back configuration.

A single impeller is defined by an impeller width and diameter along with at least two performance points having the same suction state and impeller speed. Performance points sharing the same suction state and impeller speed form a performance curve. Each point is defined by a suction state and a chosen combination of other parameters such as discharge state, mass flow and speed. A suction or discharge state is defined by the working gas composition and a combination of two other parameters. For example, we can define a suction state by specifying the working gas composition together with suction pressure and temperature. Instead of specifying pressure and temperature as parameters, we have the option to choose combinations like pressure and enthalpy, density and entropy, or enthalpy and entropy.

8.1.1 Compressor testing

Expanding from a single impeller, we can define a straight-through or back-to-back compressor. This is used for compressor testing following the ASME PTC 10 standard which is a performance test code for compressors and exhausters. PTC 10 tests are called shop tests and are performed to confirm the aerodynamic compressor performance that has been contractually agreed with a compressor vendor. The code offers two alternative procedures to test centrifugal compressors:

- Test 1: A test with a gas very close in composition and thermodynamic properties to the specified (contractual) gas. Performed at pressures and power demand close to values agreed in a purchase agreement for the compressor.

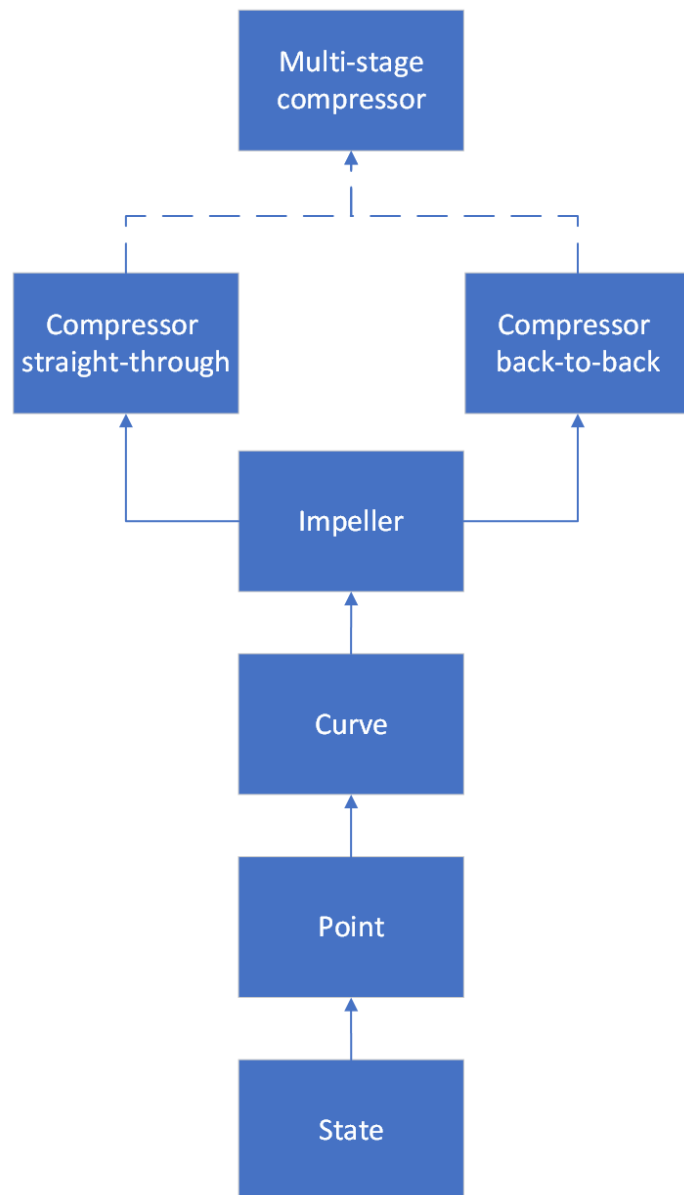


Figure 18: Flow diagram for centrifugal compressor performance code. Multi-stage compressors are not implemented yet.

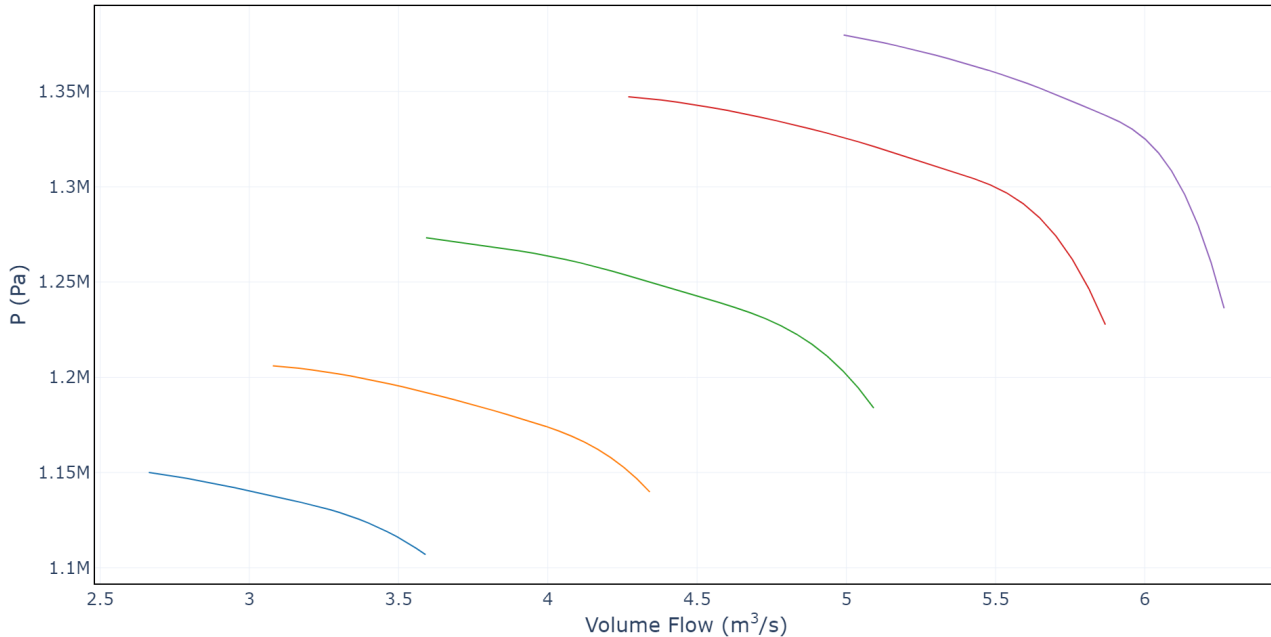


Figure 19: Impeller discharge pressure as a function of gas volume flow. The different curves correspond to different impeller speed.

- Test 2: A test using a substitute gas that is different from the specified (contractual) gas but allows to emulate the aerodynamic operating conditions, usually with an inert gas mixture like nitrogen or carbon dioxide. Performed at pressures lower than the specified conditions.

Apart from lower expenses, there are several advantages of performing a type 2 test. A key advantage of using a gas allowed by a type 2 test is that it typically is a pure or binary gas mixture with a well known thermodynamic behavior. Hence, similarity laws for turbomachinery can be taken advantage of in order to determine the performance at operating conditions on a detailed level [18].

The compressor vendor will also provide a guarantee point which is a guaranteed compressor performance point. A compressor is defined in the CCP code by a guarantee point with the specified gas of the compressor. Additionally, we must set the test gas along with different performance test points that have been acquired from a shop test. The code will then create Impeller instances and calculate the expected performance at the specified conditions. Through this approach, we can generate the performance map of a hydrogen compressor by collecting test data from physical compressor tests conducted with a less hazardous gas at lower pressures. Properties such as the discharge pressure, head and efficiency can be plotted against volume flow at the compressor inlet and outlet. These properties can also be plotted at the inlet and outlet of each individual impeller in the compressor. Moreover, given an Impeller instance it is possible to convert the impeller into having a different suction state.

Another capability of the CCP code is to import a graphical performance map via Engauge Digitizer [19]. This will extract performance points from the performance map making it possible to create an impeller or a full compressor from these points. This has been done in Figure 19 where the discharge pressure of an impeller is plotted against volume flow for different impeller speeds. The gas consists of 90% H₂ and 10% CO₂. A tutorial to Engauge Digitizer can be found at

ccp-centrifugal-compressor-performance.readthedocs.io/en/stable/user_guide/engauge.html.



SINTEF

8.2 Polytropic methods

The calculation of head and efficiency for a performance point is carried out by assuming a polytropic compression process. The polytropic compression will, as discussed in section 5, lie between an isotropic and an isothermal compression in terms of required compression work. However, there are several methods used to calculate the polytropic head and efficiency. The default polytropic method is Schultz, which is the method adopted by the ASME PTC 10 standard. Other available methods are Mallen-Saville, Huntington and Sandberg-Colby. The gas properties calculations necessary to determine the polytropic compression process is performed by Thermopack and Thermphys. Both Thermopack and Thermphys make use of an equation of state which describes the state of the gas under a given set of physical conditions like pressure, temperature and volume. Some of the available equations of state are NIST-MEOS, Cubic SRK and SAFT-VR. Tests of the code have been performed against the

Compressor efficiency is also affected by heat loss through the casing. This can be accounted for by setting e.g. the casing temperature and area. Several other parameters can be set such as seal gas temperature, oil temperature and ambient temperature.



SINTEF

9 Conclusion and further work

Since hydrogen is a very small molecule, hydrogen gas has a low volumetric energy density, and is also difficult to compress. Replacing natural gas by hydrogen while delivering the same amount of energy will therefore require novel hydrogen compressors with high discharge pressure and large flow rate. This demand becomes even more pronounced in the context of Norwegian hydrogen exports, owing to the extensive distances over which hydrogen must be transported. Hence, centrifugal compressors are anticipated to play a vital role in the compression of hydrogen for export, as they can achieve high discharge pressures and large flow rates while demanding comparatively lower maintenance than reciprocating compressors. In order to attain the required high discharge pressures, it is necessary to operate the impellers at elevated speeds. This presents a notable challenge in terms of the material strength limitations of the impeller that must be effectively addressed. On a contrasting note, hydrogen's high speed of sound mitigates some of the issues associated with high Mach numbers, a concern that is more pronounced when dealing with compressors using gases with higher molar weight as the working fluid.

The export of hydrogen from Norway may necessitate discharge pressures of approximately 200 bar and flow rates reaching around 300 t/h. Unfortunately, the open literature offers limited detailed information on centrifugal compressors designed to meet these performance criteria. Nevertheless, it is worth noting ongoing initiatives like the BarMar project, which aims to transport hydrogen across a distance of 455 km via pipelines, maintaining a pressure of 210 bar and a capacity of 228 t/h. For lower flow rates and discharge pressures, several compressor alternatives have been proposed. Among these alternatives, a six-stage centrifugal compressor concept has been designed in accordance with objectives put forward by the US Department of Energy. It compresses hydrogen from 24 bar up to 69 bar while having a flow rate of up to 40 t/h.

In order to investigate the performance and optimal configurations of centrifugal compressors, a specialized centrifugal compressor performance code has been documented for future research and development. This code offers the capability to configure and analyze centrifugal compressors, enabling users to specify parameters like impeller dimensions, gas composition and rotational speed. Additionally, the code can import compressor performance maps and be used in compressor testing in accordance with the ASME PTC 10 standard. Currently, the code supports the definition of either a single-section straight-through compressor or a two-section compressor in a back-to-back arrangement. Ongoing development will focus on expanding its capabilities to model multi-stage compressors with intercooling. Notably, a user-friendly web app for factory testing has recently been implemented using this code, offering an accessible interface for those who prefer not to delve into the underlying Python code.

Given the limited availability of detailed information on high-capacity centrifugal compressors in the open literature, obtaining information directly from vendors regarding their products, especially data from performance testing of prototypes, is still a necessary step in the research process. The work described in this memo will be continued in WP 2.3 of FME HYDROGENi in 2024.

References

- [1] Mohammad-Reza Tahan. Recent advances in hydrogen compressors for use in large-scale renewable energy integration. *International Journal of Hydrogen Energy*, 47(83):35275–35292, October 2022.
- [2] P.G. Hill and C.R. Peterson. *Mechanics and thermodynamics of propulsion*. Addison-Wesley, 1992. tex.lccn: 91004691.
- [3] L. F. Schumann, D. A. Clark, and J. R. Wood. Effect of area ratio on the performance of a 5.5:1 pressure ratio centrifugal impeller. *Journal of Turbomachinery*, 109(1):10–19, January 1987.
- [4] E. Tzimas, C. Filiou, Stathis Peteves, and J.-B Veyret. Hydrogen storage: State of the art and future persepective. Technical Report cat. No. LD-NA-20995-EN-C, European Commision Joint Research Centre, January 2003.
- [5] C. Tsiklios, M. Hermesmann, and T. E. Müller. Hydrogen transport in large-scale transmission pipeline networks: Thermodynamic and environmental assessment of repurposed and new pipeline configurations. *Applied Energy*, 327:120097, December 2022.
- [6] Simona Cerniauskas, Antonio Jose Chavez Junco, Thomas Grube, Martin Robinius, and Detlef Stolten. Options of natural gas pipeline reassignment for hydrogen: Cost assessment for a Germany case study. *International Journal of Hydrogen Energy*, 45(21):12095–12107, April 2020.
- [7] Anthony Wang, Kees van der Leun, Daan Peters, and Maud Buseman. European Hydrogen Backbone: How a dedicated hydrogen Infrastructure can be created. Technical report, 2020.
- [8] NORSOK P-002:2014. Technical report, Standards Norway, 2014.
- [9] Hooshang Heshmat, Zhaohui Ren, Andrew Hunsberger, Said Jahanmir, and James Walton. *Oil-Free Foil Bearings and Seals for Centrifugal Hydrogen Compressor*, volume 8. October 2011. Journal Abbreviation: Tribology Online Publication Title: Tribology Online.
- [10] Di Bella and Francis A. Development Of A Centrifugal Hydrogen Pipeline Gas Compressor. Technical Report TM-1785, Concepts ETI, Inc. dba Concepts NREC, April 2015.
- [11] Néstor González Díez, Simone van der Meer, Jorge Bonetto, and Arend Herwijn. Technical assessment of Hydrogen transport, compression, rocessing offshore. Technical Report NSE3-D3.1, North Sea Energy, June 2020.
- [12] Andrzej Witkowski, Andrzej Rusin, Mirosław Majkut, and Katarzyna Stolecka. Comprehensive analysis of hydrogen compression and pipeline transportation from thermodynamics and safety aspects. *Energy*, 141:2508–2518, December 2017.
- [13] Kevin Topolski, Evan P. Reznicek, Burcin Cakir Erdener, Chris W. San Marchi, Joseph A. Ronevich, Lisa Fring, Kevin Simmons, Omar Jose Guerra Fernandez, Bri-Mathias Hodge, and Mark Chung. Hydrogen Blending into Natural Gas Pipeline Infrastructure: Review of the State of Technology. Technical Report NREL/TP-5400-81704, National Renewable Energy Lab. (NREL), Golden, CO (United States), October 2022.
- [14] Petróleo Brasileiro S.A. ccp, 2022.

- [15] Ian H. Bell, Jorrit Wronski, Sylvain Quoilin, and Vincent Lemort. Pure and pseudo-pure fluid thermophysical property evaluation and the open-source thermophysical property library CoolProp. *Industrial & Engineering Chemistry Research*, 53(6):2498–2508, 2014. tex.eprint: <http://pubs.acs.org/doi/pdf/10.1021/ie4033999>.
- [16] E. W. Lemmon, I. H. Bell, M. L. Huber, and M. O. McLinden. NIST standard reference database 23: Reference fluid thermodynamic and transport properties-REFPROP, version 10.0, national institute of standards and technology, 2018.
- [17] SINTEF Energy Research and NTNU Department of Chemistry. Thermopack.
- [18] Klaus Brun and Rainer Kurz. MYTH: AN ASME PTC-10 TYPE 1 IS BETTER THAN A TYPE 2 TEST. *Turbomachinery International*, October 2022.
- [19] Mark Mitchell, Baurzhan Muftakhidinov, Tobias Winchen, Alexander Wilms, Bas van Schaik, Mo-Gul, The Gitter Badger, Zbigniew Jędrzejewski-Szmek, kensington, kylesower, and badshah400. Engauge Digitizer Software, July 2020.